Characteristics and controlling factors of dispersion in bounded heterogeneous porous media

Zhiming Lu,[1] Andrew V. Wolfsberg,[1] Zhenxue Dai,[1] and Chunmiao Zheng[2]

Received 14 July 2009; revised 2 August 2010; accepted 30 September 2010; published 2 December 2010.

[1] In this study, we present first-order (in terms of the log conductivity variance) analytical solutions to displacement covariances X_{ij} and macrodispersion coefficients D_{ij} for transport of conservative solutes in two-dimensional, bounded heterogeneous porous media. These solutions are presented as infinity series and are explicit functions of the statistics of the log hydraulic conductivity. Using numerical examples, the convergence of these solutions in terms of the number of terms in truncated finite summations is first investigated, and the accuracy of these solutions is examined by comparing them with results from Monte Carlo simulations and the semianalytical solutions of Osnes (1998). Through several examples, the general features of time-dependent X_{ij} and D_{ij} are discussed. Unlike in unbounded domains, the longitudinal macrodispersivity D_{11} for bounded domains does not approach an asymptotic value at large dimensionless time but instead increases quickly near the downstream constant head boundary. In addition, D_{11} for bounded domains is always larger than that in unbounded domains, and accordingly, the transverse macrodispersivity D_{22} in bounded domains is smaller than that in unbounded domains. These differences stem from the lateral no-flow boundaries in our bounded domain models. We also investigated the effect of domain sizes on X_{ij} and D_{ij}. Our study shows that both X_{ij} and D_{ij} depend not only on the dimensionless size of the domain but also on its aspect ratio. The dependence of X_{ij} and D_{ij} on the particles' initial location has also been investigated at detail. Our results indicate that while this dependence is very small for X_{11} and D_{11}, the release location has a significant impact on both X_{22} and D_{22}. Our solutions to both displacement covariances and macrodispersivity are compared against those derived from tracer test data at the Borden site. The comparison shows that our solutions are quite close to observed data, indicating that they may be applicable to predict solute transport at the field scale.

Citation: Lu, Z., A. V. Wolfsberg, Z. Dai, and C. Zheng (2010), Characteristics and controlling factors of dispersion in bounded heterogeneous porous media, *Water Resour. Res.*, *46*, W12508, doi:10.1029/2009WR008392.

1. Introduction

[2] Accurate description of contaminant transport in heterogeneous porous media is very important for remediating contaminates in soils and aquifers. The advection-dispersion equation is the most widely used governing equation for describing solute transport in subsurface. Advection represents transport of solutes with fluid flow, while dispersion (hydrodynamic dispersion) includes mechanical and molecular diffusion. The former is caused by variations of fluid velocity in the pore space of porous media, and the latter is due to molecules' random motion. Effective dispersivity is a parameter characterizing dispersion.

[3] Dependency of effective dispersivity on travel distance (or travel time) has been a major topic in both theoretical and case studies in the last two decades. A number of case studies have been conducted to investigate the scale effect in effective dispersivity at the column scale [*Khan and Jury*, 1990; *Porro et al.*, 1993; *Zhang et al.*, 1994; *Zhang and Neuman*, 1995; *Silliman and Simpson*, 1987; *Pang and Hunt*, 2001] and the field scale [*Sauty*, 1980; *Sudicky et al.*, 1983; *Freyberg*, 1986; *Gelhar et al.*, 1992]. At the column scale, it has been observed that effective dispersivity increases with travel distance for both homogeneous and heterogeneous columns. Although some of field studies indicate inconsistent relationship between effective dispersivity and travel distance or travel time [*Leland and Hillel*, 1982; *Taylor and Howard*, 1987], most of these studies do show the dependence of effective dispersivity on travel distance from the source of solutes [*Sauty*, 1980; *Sudicky et al.*, 1983; *Freyberg*, 1986; *Gelhar et al.*, 1992]. These studies indicate that effective dispersivity increases with travel distance at early time until a characteristic value is reached, and then it remains a constant. Effective dispersivities (or macrodispersivities) estimated from field-scale tracer tests are often much larger than those measured in the laboratory for the same type of porous materials.

[4] Several theoretical efforts have been made to account for this dependence of effective dispersivity on travel time or travel distance. Most of these theories rely on the heteroge-

[1]Computational Earth Sciences Group, Los Alamos National Laboratory, Los Alamos, New Mexico, USA.
[2]Department of Geological Sciences, University of Alabama, Tuscaloosa, Alabama, USA.

0043-1397/10/2009WR008392

neous nature of the porous media. Stochastic analyses [*Gelhar et al.*, 1979; *Gelhar and Axness*, 1983; *Dagan*, 1984; *Neuman et al.*, 1987; *Dagan*, 1988; *Rubin*, 1990; *Schwarze et al.*, 2001; *Dai et al.*, 2007] usually relate macrodispersivity to the spatial correlation structure of the hydraulic conductivity of the porous media. According to these stochastic models, macrodispersivity is a function of time at the early time and will reach an asymptotic constant value after all scales of variability have been experienced. *Gelhar and Axness* [1983] conducted three-dimensional stochastic analysis of macrodispersion in heterogeneous porous media. Their analysis yields a finite asymptotic longitudinal effective dispersivity. *Neuman et al.* [1987] developed a stochastic theory of field-scale Fickian dispersion in anisotropic porous media. Their theory also shows that the field-scale longitudinal effective dispersivity reaches a nonzero constant value asymptotically. *Dagan* [1988] suggested that the travel distance required to reach asymptotic constant value is about tens of integral scales of the horizontal conductivity field.

[5] Most theoretical studies on macrodispersivities are based on the assumption that the domain of interest is unbounded. It has been shown that the boundary effect is very small if the domain is sufficient large comparing to the correlation scales and/or if the solute transport occurs in regions that are at least several to tens of correlation lengths away from the boundary. However, it is not uncommon in literature that those stochastic theories developed for unbounded domains were applied directly to some field or experimental studies where the domain size was as small as a few correlation scales [*Keller et al.*, 1995]. This is because there is no handy analytical solution available to effective dispersivity for bounded, randomly heterogeneous conductivity fields.

[6] *Osnes* [1998] derived analytical solutions to velocity moments for steady state uniform mean flow in rectangular domains with an isotropic separable exponential covariance of the log hydraulic conductivity. The solute displacement covariances X_{ij} were expressed as integrals of the velocity covariances, which need to be evaluated numerically. Expressions for macrodispersivities were not given. In this study, on the basis of first-order analytical solutions of velocity covariance functions in two-dimensional bounded heterogeneous porous media [*Lu and Zhang*, 2005], we derived analytical expressions for displacement covariances X_{ij} and macrodispersion coefficients D_{ij} (or macrodispersivities) under assumptions that the mean flow is uniform and that the covariance of the conductivity field is anisotropic separable exponential. These solutions are presented as infinite series and are much concise than Osnes's solutions [*Osnes*, 1998].

[7] Because these analytical solutions are accurate only up to first order in terms of the log conductivity variance (or second order in the standard deviation of the log conductivity), Monte Carlo simulations have been conducted to assess their accuracy. Our solutions were also compared with those of *Osnes* [1998] and *Dagan* [1984] for the case presented by *Osnes* [1998]. We then discussed the general characteristics of our first-order solutions, including the difference from their counterparts for unbounded domains and the dependence of displacement covariances and macrodispersivities on the travel distance or travel time. In particular, the effects of the domain aspect ratio and the particles' release location on X_{ij} and D_{ij} have been investigated at detail.

[8] The analytical solutions presented in this study provide a rigorous means to explore the characteristics of dispersive transport in bounded, randomly heterogeneous porous media under uniform mean flow conditions, and to quantify the sensitivity of the scale-dependent effective dispersivity to key parameters of the porous media, including the variance of log hydraulic conductivity, correlation scales, domain geometry, and relative source location.

2. Mathematical Development

[9] We consider steady state saturated flow in two-dimensional, bounded, randomly heterogeneous porous media governed by the following equation

$$\nabla \cdot [K_s(\mathbf{x})\nabla h(\mathbf{x})] = 0, \quad \mathbf{x} \in \Omega = [0, L_1] \times [0, L_2], \tag{1}$$

where h is the hydraulic head, K_s is the saturated hydraulic conductivity, $\mathbf{x} = (x_1, x_2)^T$ is the vector of Cartesian coordinates, and L_1 and L_2 are lengths of the simulation domain in x_1 and x_2 directions, respectively. The boundary conditions associated with (1) are given as

$$h(x_1 = 0, x_2) = H_1, \; h(x_1 = L_1, x_2) = H_2, \tag{2}$$

$$\left.\frac{\partial h(\mathbf{x})}{\partial x_2}\right|_{x_2=0} = 0, \quad \left.\frac{\partial h(\mathbf{x})}{\partial x_2}\right|_{x_2=L_2} = 0, \tag{3}$$

where the prescribed head H_1 and H_2 are assumed to be deterministic constants. Without loss of generality, it is assumed $H_1 > H_2$, and the mean flow is in the x_1 direction.

[10] It is assumed that the hydraulic conductivity K_s is a spatially correlated random function. In this case, the hydraulic head in (1)–(3) is also a random quantity, and thus these equations become stochastic. A number of methods have been developed to solve stochastic equations, including Monte Carlo simulations, moment equation methods [e.g., *Guadagnini and Neuman*, 1999a, 1999b], moment methods based on Karhunen-Loève decomposition [*Zhang and Lu*, 2004], spectral methods [*Yeh et al.*, 1985; *Li and McLaughlin*, 1991], and probability collocation methods [*Li and Zhang*, 2007; *Li et al.*, 2009]. For this particular problem, velocity moments (mean and covariance) can be solved analytically, providing the covariance structure of the conductivity is separable exponential [*Osnes*, 1995; *Lu and Zhang*, 2005]. In sections 2.1–2.3, for completeness we first give the autocovariance of velocity fields as in the work by *Lu and Zhang* [2005], we then derive analytical solutions to displacement covariances and macrodispersivities.

2.1. Velocity Covariance

[11] The flux in porous media is related to the hydraulic head and the hydraulic conductivity by Darcy's law:

$$\mathbf{q}(\mathbf{x}) = -K_s(\mathbf{x})\nabla h(\mathbf{x}). \tag{4}$$

Following the moment methods, we assume that the hydraulic conductivity follows a lognormal distribution, and work with the log-transformed variable $Y(\mathbf{x}) = \ln[K_s(\mathbf{x})] = \langle Y(\mathbf{x})\rangle + Y'(\mathbf{x})$, where $\langle Y(\mathbf{x})\rangle$ and $Y'(\mathbf{x})$ are the mean and the zero mean perturbation of the log hydraulic conductivity, respectively. Accordingly, the hydraulic head and flux may be formally decomposed as $h(\mathbf{x}) = h^{(0)}(\mathbf{x}) + h^{(1)}(\mathbf{x}) + \ldots$ and $\mathbf{q}(\mathbf{x}) = \mathbf{q}^{(0)}(\mathbf{x}) + \mathbf{q}^{(1)}(\mathbf{x}) + \cdots$, where numbers in the superscripts stand for the

order in terms of σ_Y, the standard deviation of the log hydraulic conductivity.

[12] Substituting decompositions of $h(\mathbf{x})$, $\mathbf{q}(\mathbf{x})$, and $K_s(\mathbf{x}) = \exp(Y(\mathbf{x})) \approx K_G[1 + Y'(\mathbf{x})]$, where K_G is the geometric mean of hydraulic conductivity, into (4) and collecting terms at different orders, for the zeroth order, one has $q_1^{(0)}(\mathbf{x}) = K_G J$, and $q_2^{(0)}(\mathbf{x}) = 0$, where $J = (H_1 - H_2)/L_1$ is the steady state mean hydraulic gradient. The first-order flux can be written as

$$q_i^{(1)}(\mathbf{x}) = -K_G \frac{\partial h^{(1)}(\mathbf{x})}{\partial x_i} + Y'(\mathbf{x}) q_i^{(0)}(\mathbf{x}), \quad i = 1, 2. \tag{5}$$

From this equation one can approximate the flux covariance $q_{ij}(\mathbf{x}, \mathbf{y}) = \langle q_i^{(1)}(\mathbf{x}) q_j^{(1)}(\mathbf{y}) \rangle$, $i, j = 1, 2$, as

$$q_{ij}(\mathbf{x}, \mathbf{y}) = K_G^2 \frac{\partial^2 C_h(\mathbf{x}, \mathbf{y})}{\partial x_i \partial y_j} - K_G q_j^{(0)}(\mathbf{y}) \frac{\partial C_{Yh}(\mathbf{y}, \mathbf{x})}{\partial x_i} - K_G q_i^{(0)}(\mathbf{x}) \frac{\partial C_{Yh}(\mathbf{x}, \mathbf{y})}{\partial y_j} + q_i^{(0)}(\mathbf{x}) q_j^{(0)}(\mathbf{y}) C_Y(\mathbf{x}, \mathbf{y}). \tag{6}$$

Note that the flux covariance is accurate to the first order in terms of the log conductivity variance (or second order in terms of the standard deviation of the log conductivity). The velocity covariance can be readily formulated from flux covariance using a simple relationship $u_{ij}(\mathbf{x}, \mathbf{y}) = q_{ij}(\mathbf{x}, \mathbf{y})/\phi^2$, where ϕ is the porosity of the porous media. For simplicity, we treat porosity as a deterministic constant due to its relatively small variability, although *Riva et al.* [2008] recently showed that the variability of porosity was important in interpreting a forced gradient tracer test.

[13] For an anisotropic separable exponential covariance function

$$C_Y(\mathbf{x}, \mathbf{x}') = \sigma_Y^2 \rho_Y(x_1, x_2; x_1', x_2') = \sigma_Y^2 \exp\left(-\frac{|x_1 - x_1'|}{\lambda_1} - \frac{|x_2 - x_2'|}{\lambda_2}\right), \tag{7}$$

where σ_Y^2 is the variance of the log conductivity, and λ_1 and λ_2 are the correlation lengths of Y in x_1 and x_2 directions, respectively, the autocovariance of the head, $C_h(\mathbf{x}, \mathbf{y})$, and the cross covariance between the head and the log hydraulic conductivity, $C_{Yh}(\mathbf{x}, \mathbf{y})$, can be derived analytically. The dimensionless steady state velocity covariances can be written as [*Lu and Zhang*, 2005]:

$$\frac{u_{11}(\mathbf{x}, \mathbf{y})}{U^2 \sigma_Y^2} = 16 \sum_{\substack{m,m_1=1 \\ n,n_1=0}}^{\infty} \frac{a_n \alpha_m^2 \cos(\alpha_m x_1) \cos(\beta_n x_2)}{\alpha_m^2 + \beta_n^2} \times \frac{a_{n_1} \alpha_{m_1}^2 \cos(\alpha_{m_1} y_1) \cos(\beta_{n_1} y_2)}{(\alpha_{m_1}^2 + \beta_{n_1}^2)} Q_{m_1 n_1}^{mn} - 4 \sum_{\substack{m=1 \\ n=0}}^{\infty} \frac{a_n \alpha_m^2}{\alpha_m^2 + \beta_n^2} \left[R_{mn}(\mathbf{x}) \cos(\alpha_m y_1) \cos(\beta_n y_2) + R_{mn}(\mathbf{y}) \cos(\alpha_m x_1) \cos(\beta_n x_2)\right] + \rho_Y(\mathbf{x}, \mathbf{y}), \tag{8}$$

$$\frac{u_{12}(\mathbf{x}, \mathbf{y})}{U^2 \sigma_Y^2} = -16 \sum_{\substack{m,m_1=1 \\ n,n_1=0}}^{\infty} \frac{a_n \alpha_m^2 \cos(\alpha_m x_1) \cos(\beta_n x_2)}{\alpha_m^2 + \beta_n^2} \cdot \frac{a_{n_1} \alpha_{m_1} \beta_{n_1} \sin(\alpha_{m_1} y_1) \sin(\beta_{n_1} y_2)}{\alpha_{m_1}^2 + \beta_{n_1}^2} Q_{m_1 n_1}^{mn} + 4 \sum_{\substack{m=1 \\ n=0}}^{\infty} \frac{a_n \alpha_m \beta_n}{\alpha_m^2 + \beta_n^2} R_{mn}(\mathbf{x}) \sin(\alpha_m y_1) \sin(\beta_n y_2), \tag{9}$$

$$\frac{u_{22}(\mathbf{x}, \mathbf{y})}{U^2 \sigma_Y^2} = 16 \sum_{\substack{m,m_1=1 \\ n,n_1=0}}^{\infty} \frac{a_n \alpha_m \beta_n \sin(\alpha_m x_1) \sin(\beta_n x_2)}{\alpha_m^2 + \beta_n^2} \cdot \frac{a_{n_1} \alpha_{m_1} \beta_{n_1} \sin(\alpha_{m_1} y_1) \sin(\beta_{n_1} y_2)}{\alpha_{m_1}^2 + \beta_{n_1}^2} Q_{m_1 n_1}^{mn}, \tag{10}$$

where $U = K_G J/\phi$ is the mean velocity in the mean flow direction (the x_1 direction), $\alpha_m = m\pi/L_1$, $m = 1, 2, \cdots$, $\beta_n = n\pi/L_2$, $n = 0, 1, 2, \ldots$, $a_n = 1$ for $n > 0$ and $a_n = 1/2$ for $n = 0$. The terms R_{mn} and $Q_{m_1 n_1}^{mn}$ in (8)–(10) are given as

$$R_{mn}(\mathbf{x}) = \frac{(\lambda_1/L_1)(\lambda_2/L_2)}{(\alpha_m^2 \lambda_1^2 + 1)(\beta_n^2 \lambda_2^2 + 1)} \cdot \left[2\cos(\alpha_m x_1) - e^{-x_1/\lambda_1} - (-1)^m e^{(x_1 - L_1)/\lambda_1}\right] \times \left[2\cos(\beta_n x_2) - e^{-x_2/\lambda_2} - (-1)^n e^{(x_2 - L_2)/\lambda_2}\right], \tag{11}$$

and

$$Q_{m_1 n_1}^{mn} = \frac{(\lambda_1/L_1)(\lambda_2/L_2)}{(\alpha_{m_1}^2 \lambda_1^2 + 1)(\beta_{n_1}^2 \lambda_2^2 + 1)} \cdot \left[\delta_{mm_1} + \frac{\lambda_1/L_1}{\alpha_m^2 \lambda_1^2 + 1}\left[1 + (-1)^{m+m_1}\right]\left[(-1)^m e^{-\frac{L_1}{\lambda_1}} - 1\right]\right] \times \left[\delta_{nn_1} + \delta_{n0}\delta_{n_1 0} + \frac{\lambda_2/L_2}{\beta_n^2 \lambda_2^2 + 1}\left(1 + (-1)^{n+n_1}\right] \cdot \left[(-1)^n e^{\frac{-L_2}{\lambda_2}} - 1\right)\right], \tag{12}$$

where δ_{ij} is the Kronecker delta function, $\delta_{ij} = 1$ for $i = j$, and $\delta_{ij} = 0$ otherwise. Note that both R_{mn} and $Q_{m_1 n_1}^{mn}$ are dimensionless. It is also worthy to note that $Q_{m_1 n_1}^{mn}$ has several important features. First, $Q_{m_1 n_1}^{mn}$ is symmetric in terms of its superscripts and subscripts, i.e., $Q_{m_1 n_1}^{mn} = Q_{mn}^{m_1 n_1}$. Furthermore, $Q_{m_1 n_1}^{mn}$ depends on the dimensionless domain size $l_i = L_i/\lambda_i$ rather than its actual size L_i. Finally, $Q_{m_1 n_1}^{mn} = 0$ if either $m + m_1$ or $n + n_1$ is an odd number, which allows us to compute $Q_{m_1 n_1}^{mn}$ with significantly reduced computational efforts.

[14] The expression for u_{21} has been omitted, because of the fact that $u_{21}(\mathbf{x}, \mathbf{y}) \equiv u_{12}(\mathbf{y}, \mathbf{x})$. Discussions on features of velocity covariance u_{ij} will be skipped here, because they have been discussed at sufficient detail by *Salandin and Fiorotto* [1998] based on Monte Carlo simulations and by *Osnes* [1998] using his analytical solutions. Note that even if the log hydraulic conductivity Y is stationary, the velocity field in general is nonstationary and the two-point velocity covariances $u_{ij}(\mathbf{x}, \mathbf{y})$ depend on locations $\mathbf{x}$ and $\mathbf{y}$, not just on the lag distance between these two points.

[15] Since both R_{mn} and $Q^{mn}_{m_1n_1}$ are dimensionless, it is easy to show from (8)–(10) that velocity covariances are functions of aspect ratio $\epsilon = L_2/L_1$, not just the dimensionless domain size $l_i = L_i/\lambda_i$.

2.2. Displacement Covariances

[16] For a particle originating from location $\mathbf{x}_0 = (x_{01}, x_{02})^T$ at $t = 0$, its trajectory is described by the following kinematic equation:

$$\frac{d\mathbf{X}(t;\mathbf{x}_0)}{dt} = \mathbf{u}[\mathbf{X}(t;\mathbf{x}_0)], \tag{13}$$

subject to initial condition $\mathbf{X}(0;\mathbf{x}_0) = \mathbf{x}_0$, where $\mathbf{X}(t;\mathbf{x}_0)$ stands for particle's position at time t and $\mathbf{u}[\mathbf{X}(t;\mathbf{x}_0)]$ denotes the velocity of the particle at t. When the velocity $u_i(\mathbf{x}, t)$ is a random space function, so is the particle's position.

[17] In this study, it is assumed that the effect of local dispersion is relatively small and can be ignored. This assumption has been widely used in many studies [*Dagan*, 1987; *Bellin et al.*, 1992; *Dagan*, 1994; *Hsu et al.*, 1996; *Salandin and Fiorotto*, 1998; *Osnes*, 1998]. In fact, *Zhang and Neuman* [1996] investigated the effect of local dispersion and found that it does not have a significant impact on transport behavior. *Fiori* [1996, 1998] also found that local dispersion has no significant effect on the asymptotic longitudinal macrodispersion. Although most of these studies concerned unbounded domains, it is reasonable to assume that the effect of local dispersion should also be small for bounded domains.

[18] Let us denote $\mathbf{X}(t;\mathbf{x}_0)$ as $\mathbf{X}_t$ when there is no confusion, and formally decompose $\mathbf{X}_t$ in terms of the order of σ_Y as $\mathbf{X}_t = \mathbf{X}_t^{(0)} + \mathbf{X}_t^{(1)} + \ldots$. By substituting this expression and the decomposition of u_i into (13) and collecting terms at separate orders, one derives equations for $\mathbf{X}_t^{(n)}$, $n = 1, 2, \ldots$. In particular, the first-order perturbation of particle's position for the case of unidirectional uniform mean flow can be written as [*Osnes*, 1998; *Lu and Zhang*, 2003]:

$$X^{(1)}_{t,i} = \int_0^t u_i^{(1)}\left(\mathbf{X}^{(0)}_{t'}\right)dt'. \tag{14}$$

From this equation one can formulate the first-order (in terms of log conductivity variance) displacement covariance as

$$\begin{aligned} X_{ij}(t) &= \left\langle X^{(1)}_{t,i} X^{(1)}_{t,j}\right\rangle \\ &= \int_0^t\int_0^t u_{ij}\left(\mathbf{X}^{(0)}_{t'};\mathbf{X}^{(0)}_{t''}\right)dt'dt'' \\ &= \int_0^t\int_0^t u_{ij}(x_{01}+Ut', x_{02}; x_{01}+Ut'', x_{02})dt'dt''. \end{aligned} \tag{15}$$

Because the velocity field in bounded domains is nonstationary, the integrand in (15) cannot be reduced to $u_{ij}(U(t'-t''), 0)$ as in the case of infinite domains. *Osnes* [1998] gave a similar expression for X_{ij} as an integral of velocity covariances but did not go further to provide explicit expressions for X_{ij} and D_{ij}, because his expressions for velocity covariances are relatively complicated. Our concise expressions for velocity covariances allow us to derive X_{ij} and D_{ij} explicitly. Substituting u_{ij} in (8)–(10) into (15) and integrating the resultant expressions yield

$$\begin{aligned} \frac{X_{11}}{\lambda_1^2\sigma_Y^2} &= \frac{16l_1^2\epsilon^4}{\pi^2}\sum_{\substack{m,m_1=1\\ n,n_1=0}}^{\infty}\frac{ma_n\cos(\beta_n x_{02})S_m(t)}{m^2\epsilon^2+n^2} \\ &\quad\cdot\frac{m_1 a_{n_1}\cos(\beta_{n_1}x_{02})S_{m_1}(t)}{m_1^2\epsilon^2+n_1^2}\;Q^{mn}_{m_1n_1} \\ &\quad-\frac{8l_1\epsilon^2}{\pi}\sum_{\substack{m=1\\ n=0}}^{\infty}\frac{ma_n}{m^2\epsilon^2+n^2}\cos(\beta_n x_{02})S_m(t)\;G_{mn}(t) \\ &\quad+2\left[\frac{Ut}{\lambda_1}-1+e^{-Ut/\lambda_1}\right], \end{aligned} \tag{16}$$

$$\begin{aligned} \frac{X_{12}}{\lambda_1^2\sigma_Y^2} &= -\frac{16l_1^2\epsilon^3}{\pi^2}\sum_{\substack{m,m_1=1\\ n,n_1=0}}^{\infty}\frac{ma_n\cos(\beta_n x_{02})S_m(t)}{m^2\epsilon^2+n^2} \\ &\quad\cdot\frac{n_1 a_{n_1}\sin(\beta_{n_1}x_{02})C_{m_1}(t)}{m_1^2\epsilon^2+n_1^2}\;Q^{mn}_{m_1n_1} \\ &\quad+\frac{4l_1\epsilon}{\pi}\sum_{m,n=1}^{\infty}\frac{n}{m^2\epsilon^2+n^2}\sin(\beta_n x_{02})S_m(t)G_{mn}(t), \end{aligned} \tag{17}$$

and

$$\begin{aligned} \frac{X_{22}}{\lambda_1^2\sigma_Y^2} &= \frac{16l_1^2\epsilon^2}{\pi^2}\sum_{\substack{m,m_1=1\\ n,n_1=1}}^{\infty}\frac{n\sin(\beta_n x_{02})C_m(t)}{m^2\epsilon^2+n^2} \\ &\quad\times\frac{n_1\sin(\beta_{n_1}x_{02})C_{m_1}(t)}{m_1^2\epsilon^2+n_1^2}\;Q^{mn}_{m_1n_1} \end{aligned} \tag{18}$$

where $l_i = L_i/\lambda_i$, $i = 1, 2$, are dimensionless domain sizes, $\epsilon = L_2/L_1$ is the aspect ratio of the domain, and some additional terms are defined as

$$S_m(t) = \sin[\alpha_m(x_{01}+Ut)] - \sin(\alpha_m x_{01}), \tag{19}$$

$$C_m(t) = \cos(\alpha_m x_{01}) - \cos[\alpha_m(x_{01}+Ut)], \tag{20}$$

and

$$\begin{aligned} G_{mn}(t) &= \frac{(\lambda_1/L_1)(\lambda_2/L_2)}{(\alpha_m^2\lambda_1^2+1)(\beta_n^2\lambda_2^2+1)} \\ &\quad\cdot\left[2\cos(\beta_n x_{02}) - e^{-x_{02}/\lambda_2} - (-1)^n e^{(x_{02}-L_2)/\lambda_2}\right] \\ &\quad\times\left[\frac{2S_m(t)}{\alpha_m\lambda_1} - \left(e^{-\frac{x_{01}}{\lambda_1}} + (-1)^m e^{\frac{x_{01}+Ut-L_1}{\lambda_1}}\right)\left(1-e^{-\frac{Ut}{\lambda_1}}\right)\right]. \end{aligned} \tag{21}$$

Note that X_{21} is the same as X_{12} and has been omitted. It should be emphasized that in general, the dimensionless displacement covariances depend not only on the dimensionless domain size l_i, $i = 1, 2$, but also on the domain aspect ratio $\epsilon = L_2/L_1$. Only in the case of isotropic hydraulic conductivity fields can the dimensionless displacement covariances be presented in terms of the dimensionless domain size

alone, because of the fact that $\epsilon = L_2/L_1 = (L_2/\lambda)/(L_1/\lambda) = l_2/l_1$ in this particular case.

2.3. Macrodispersion Coefficients

[19] Once the expressions for solute displacement covariances X_{ij} are found, the macrodispersion coefficients D_{ij} can be derived easily using $D_{ij} = (1/2)dX_{ij}/dt$. For D_{11} and D_{22}, one has

$$\frac{D_{11}}{\lambda_1 U\sigma_Y^2} = \frac{8l_1\epsilon^4}{\pi}\sum_{\substack{m,m_1=1\\ n,n_1=0}}^{\infty}\frac{mm_1a_na_{n_1}Q_{m_1n_1}^{mn}\cos(\beta_n x_{02})\cos(\beta_{n_1}x_{02})}{(m^2\epsilon^2+n^2)(m_1^2\epsilon^2+n_1^2\sigma^2)} \times\left[m\cos(\alpha_m x_1)S_{m_1}(t)+m_1\cos(\alpha_{m_1}x_1)S_m(t)\right] - \frac{4l_1\epsilon^2}{\pi}\sum_{\substack{m=1\\ n=0}}^{\infty}\frac{ma_n\cos(\beta_n x_{02})}{m^2\epsilon^2+n^2} \cdot\left[\alpha_m\lambda_1\cos(\alpha_m x_1)G_{mn}(t)+S_m(t)R_{mn}(x_1;x_{02})\right] + \left[1-e^{-Ut/\lambda_1}\right], \quad (22)$$

$$\frac{D_{22}}{\lambda_1 U\sigma_Y^2} = \frac{8l_1\epsilon^2}{\pi}\sum_{\substack{m,m_1=1\\ n,n_1=1}}^{\infty}\frac{nn_1\sin(\beta_n x_{02})\sin(\beta_{n_1}x_{02})Q_{m_1n_1}^{mn}}{(m^2\epsilon^2+n^2)(m_1^2\epsilon^2+n_1^2)} \times\left[m\sin(\alpha_m x_1)C_{m_1}(t)+m_1\sin(\alpha_{m_1}x_1)C_m(t)\right], \quad (23)$$

where $x_1 = x_{01} + Ut$, and all other terms have been defined previously. Since (22) and (23) have been normalized by the mean velocity U, they can also be considered as dimensionless macrodispersivities.

3. Numerical Examples

[20] In this section, we first examine the convergence of the derived analytical solutions of solute displacement covariances and macrodispersivities. Because the solutions to X_{ij} and D_{ij} are presented by infinite series (double or fourfold summations), they have to be truncated into finite summations, and therefore it is important to investigate the convergence of these solutions in terms of the number of terms retained in finite summations. The accuracy of the first-order analytical solutions is investigated by comparing the solutions with those of Monte Carlo simulations and semianalytical solutions of *Osnes* [1998].

[21] Once the convergence and accuracy of the solutions are assured, we then explore some features of the solutions, such as the general patterns of time-dependent macrodispersivity, the dependence of X_{ij} and D_{ij} on the domain size, correlation lengths, and the particles' release locations.

3.1. Convergence of Solutions

[22] In the first case (case 1), we consider a rectangle domain of size $L_1 = 1{,}000$ m and $L_2 = 500$ m. The origin of the coordinator system is at the lower left corner. The constant heads are prescribed at left and right boundaries as $H_1 = 15$ m and $H_2 = 10$ m, respectively. The lateral boundaries are impermeable. The porosity of the porous medium is a constant $\phi = 0.25$ in the domain. The log hydraulic conductivity is a stationary random spatial function with $\langle Y\rangle = \langle \ln K_s\rangle = 0.0$ (geometric mean $K_G = 1.0$ m/d) and $\sigma_Y^2 = 1.0$, and it is isotropic with correlation lengths $\lambda = \lambda_1 = \lambda_2 = 50$ m, which means that the dimensionless domain sizes in two directions are $l_1 = 20$ and $l_2 = 10$, respectively. The mean gradient for this case is $J = 0.005$, which yields the first-order mean velocity $U = 0.02$ m/d. Conservative particles are released at point (0 m, 250 m). In this section, we only describe the convergence of the solutions, while the features of these solutions in terms of travel distance or travel time will be discussed later.

[23] Let N be the upper bound of indexes (m, n, m_1, and n_1) in these truncated finite summations in (16)–(18) and (22) and (23). Figure 1 illustrates dimensionless displacement variances $X'_{ii} = X_{ii}/\lambda^2\sigma_Y^2$, $i = 1, 2$, as functions of the dimensionless time (or dimensionless distance) $t' = Ut/\lambda$ for different numbers of terms $N = 5$, 10, 20, and 30, where the maximum dimensionless time is 20 for this case. It seems from Figure 1 that $N = 5$ is enough for accurately computing X_{11} and larger N does not yield noticeably different results. However, more terms ($N = 10$) are required for computing X_{22}. As mentioned previously, the actual computational cost for computing X_{ij} can be reduced by a factor of four, by recognizing the fact that $Q_{m_1n_1}^{\ mn} \equiv 0$ if either $m + m_1$ or $n + n_1$ is an odd number, which means that if a fourfold summation in (16)–(18) is truncated at $N = 10$ for all indexes, there are only 50×50 nonzero terms (rather than 10^4 terms) to be computed and added up.

[24] The reason for fast convergence of X_{11} is that compared to the rest two terms with infinity summations, the third term in (16), which does not involve any summation, is dominating. In fact, the contribution of the first two terms in (16), comparing to the magnitude of the third term, is very small in the case of relatively large domains.

[25] Figure 2 shows the dimensionless macrodispersion coefficients D_{ij} (or macrodispersivities because these coefficients have been normalized by the mean velocity U) for different numbers of terms retained in summations of (22) and (23). Similar to X_{11}, the solution to D_{11} converges faster than D_{22} does. For the former, a small N value can produce very accurate results, while $N = 20$ is needed for the latter. From the discussion, we may conclude that in general a larger N is needed for computing D_{ij} than for X_{ij}.

[26] The number of terms, N, required to obtain accurate approximations of X_{ij} and D_{ij} depends on the correlation lengths λ_1 and λ_2. For the purpose of comparison, we calculate X_{ij} and D_{ij} for a case similar to the previous one but the correlation lengths are reduced from 50 m to $\lambda_1 = \lambda_2 = \lambda = 10$ m (dimensionless domain size $L_1/\lambda_1 = 100$ and $L_2/\lambda_2 = 50$). When the correlation lengths decrease, more terms are needed to accurately represent the solutions. This conclusion is consistent with the observations by *Zhang and Lu* [2004], which stated that more terms are required to approximate head moments or flux moments if the length scale of the conductivity field decreases. In addition, similar to the previous example, X_{11} and D_{11} converge fast than X_{22} and D_{22} (not shown). For example, $N = 10$ is sufficient to achieve convergence for X_{11} and D_{11}, while $N = 30$ is needed for accurately computing both X_{22} and D_{22}.

[27] Based on our numerical results, convergence of these first-order solutions can be summarized as follows. For a fixed dimensionless domain size, in general, X_{ij} converges fast than D_{ij}, and X_{11} and D_{11} converge fast than their counterparts X_{22} and D_{22}. On the other hand, for a fixed domain

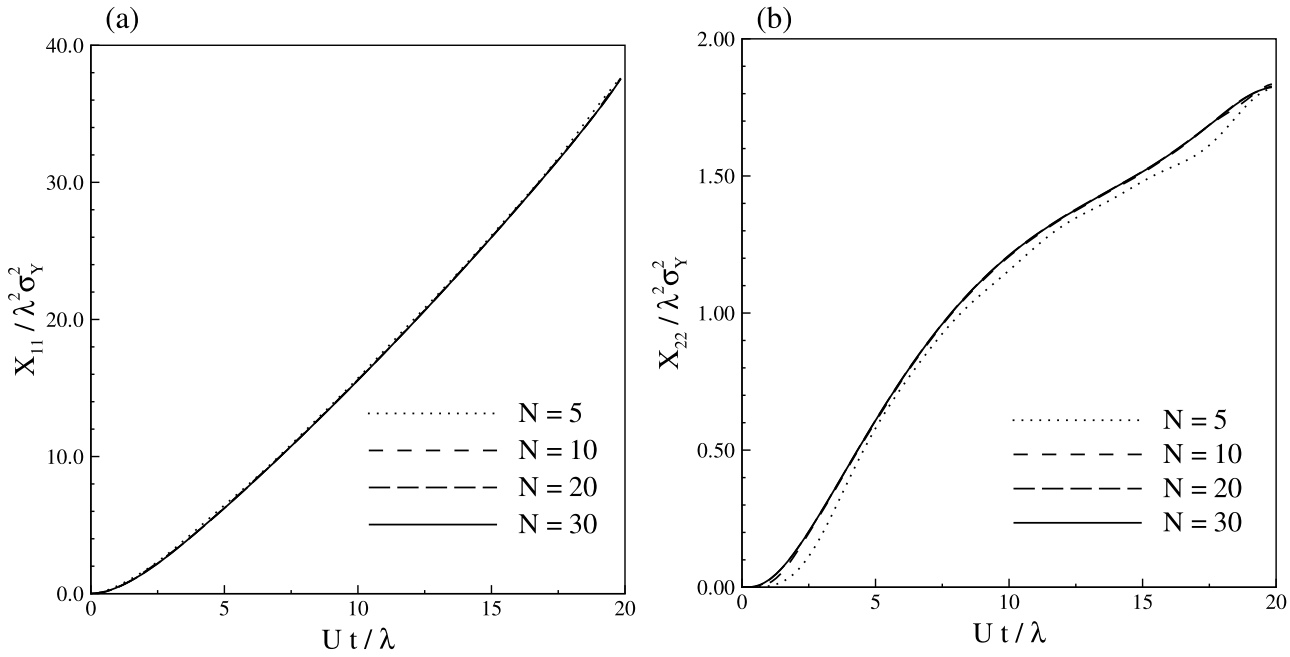

Figure 1. Convergence of time-dependent displacement covariances: (a) X_{11} and (b) X_{22} in terms of N, the number of retained terms for indexes in infinity series of (16)–(18) for the case with $\lambda = 50$ m.

size, the rate of convergence for both X_{ij} and D_{ij} decreases if the correlation lengths decrease.

3.2. Accuracy of Solutions

[28] To investigate the accuracy of the first-order analytical solutions, we conducted two different comparisons. The solutions are compared with both the Monte Carlo simulations and the semianalytical solutions of *Osnes* [1998].

3.2.1. Comparison With Monte Carlo Simulations

[29] Monte Carlo simulations (case 2) with the particle tracking method have been often used to compute displacement covariances [*Smith and Schwartz*, 1980; *Rubin*, 1990; *Bellin et al.*, 1992; *Schwarze et al.*, 2001; *Lu and Zhang*, 2003]. In this study, we conducted Monte Carlo simulations with particle tracking method in a rectangle domain of size $L_1 = 80$ m and $L_2 = 40$ m, which was uniformly discretized into 80 × 40 square elements. Similar types of boundary conditions were specified: no-flow conditions prescribed at two lateral boundaries and constant heads specified on the left and right boundaries as $H_1 = 10.5$ m and $H_2 = 10.0$ m. The mean of the log hydraulic conductivity was again given as $\langle Y \rangle = 0.0$, and the variance and the correlation lengths of the

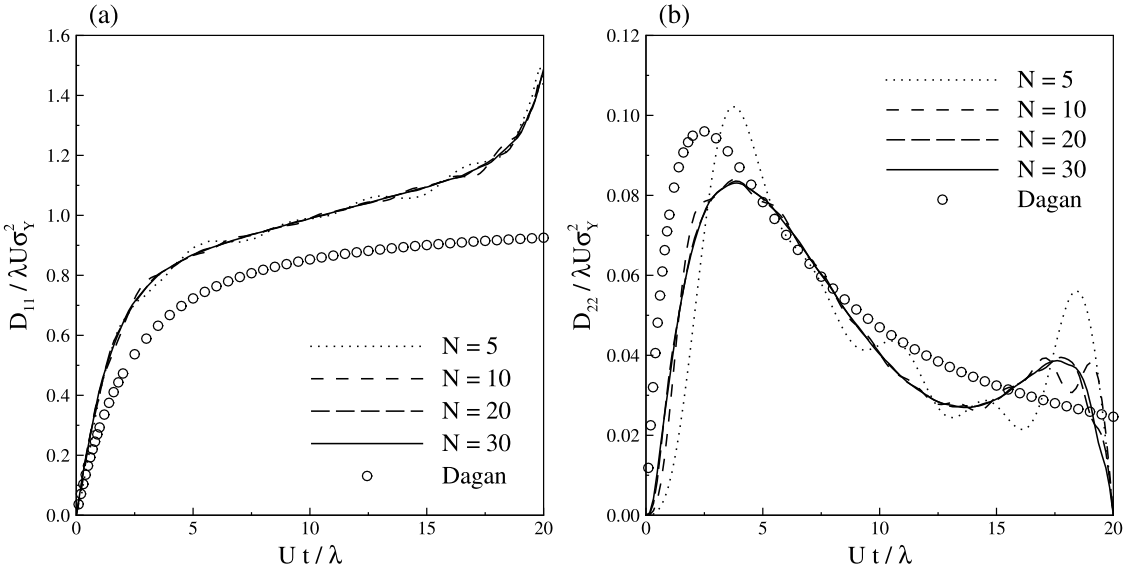

Figure 2. Convergence of time-dependent dispersivity: (a) D_{11} and (b) D_{22} in terms of N, the number of retained terms for indexes in infinity series of (22) and (23) for the case with $\lambda = 50$ m. For comparison purposes, solutions from *Dagan* [1984] for unbounded domains are also plotted.

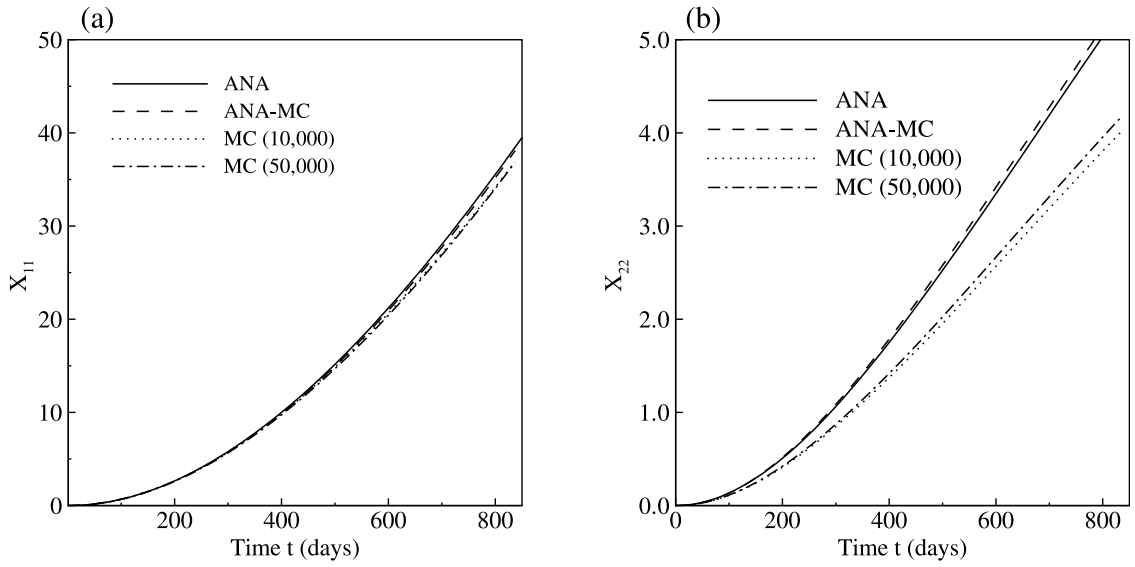

Figure 3. Comparison of time-dependent displacement covariances: (a) X_{11} and (b) X_{22} derived from Monte Carlo simulations and the first-order analytical solutions.

log hydraulic conductivity field were $\sigma_Y^2 = 0.25$ and $\lambda_1 = \lambda_2 = 10.0$ m, respectively.

[30] We first generated 50,000 two-dimensional 81 × 41 (hydraulic conductivity values being assigned at nodes rather than elements) realizations of zero mean and unit variance with a separable covariance function and given correlation lengths, using a KL-based random field generator [*Zhang and Lu*, 2004]. These zero mean, unit variance realizations were then scaled to obtain realizations with the given mean and variance.

[31] For each realization of the log hydraulic conductivity field, the corresponding velocity field was obtained by solving the steady state, saturated flow equation, i.e., (1)–(3), using the Finite Element Heat and Mass Transfer code (FEHM) [*Zyvoloski et al.*, 1997]. A conservative particle was then placed at location $(x_{01},x_{02}) = (20$ m, 20 m) and its position was recorded at some specified times until the particle left the domain. This procedure was repeated for 50,000 realizations. The particles' mean position and their spreading at any specified time were then calculated using particles' positions at that time from all Monte Carlo simulations. Because particles may leave the flow domain earlier in some Monte Carlo simulations than in others, we calculate the particle's mean position and spreading only up to the time when the fastest particle out of all 50,000 particles left the system. After that, we are not able to compute the statistics of all particles because some particles have already exit from the system. For this reason, we have chosen a relative small $\sigma_Y^2 (= 0.25)$ so that the fastest particles will not move too fast comparing to the mean position of all particles. The results from Monte Carlo simulations and those from analytical solutions are compared to assess the accuracy of first-order analytical solutions.

[32] Figure 3 compares X_{11} and X_{22} derived from analytical solutions (solid lines, ANA) and two sets of Monte Carlo (MC) simulations with 10,000 and 50,000 realizations, respectively. Figure 3 shows that the results from two sets of MC simulations are very close, which means that 50,000 realizations are sufficient for the MC method to converge. In addition, Figure 3 also demonstrates that the difference between analytical solutions and Monte Carlo results are very small for X_{11}, but relatively large for X_{22} even though the variability of log hydraulic conductivity is quite small in this case.

[33] Comparison of D_{11} and D_{22} computed from analytical solutions and the MC method are illustrated in Figure 4. Figure 4 indicates that while D_{11} from analytical solution matches well with that of Monte Carlo simulations, the discrepancy on D_{22} is relatively larger, especially at the later time, although their general patterns are similar.

[34] The difference between first-order analytical solutions and Monte Carlo results may be ascribed to several sources. First, Monte Carlo simulations may suffer from numerical errors, which depend on the numerical method and the spatial and temporal discretization. Flow or transport problems in heterogeneous porous media with small correlation lengths usually require fine spatial discretization. Monte Carlo methods also suffer from statistical errors that stem from approximating the random hydraulic conductivity field with a finite number of realizations. To reduce this type of errors, one may need to conduct a large number of simulations. The actual number of required simulations depends on the spatial variability of the process. In this example, the numerical grid used in Monte Carlo simulations is sufficiently fine (10 grids per correlation length) to reduce the effect of numerical discretization, and a considerably large number of realizations are used to reduce the statistical errors. Our results show that increasing the number of Monte Carlo simulations from 10,000 to 50,000 does improve the results a little bit, but the difference of X_{22} between MC and analytical solutions are still large. The MC results with 40,000 realizations (not shown) are almost identical to those of 50,000 realizations, which again means that 50,000 realizations are sufficiently for this case. In short, we may consider these Monte Carlo results as true solutions to X_{ij} and D_{ij}.

[35] The second possible source of errors that contributes to the difference between MC results and analytical solutions is that analytical solutions are accurate only up to first order in terms of the log conductivity variance. There are two approximations involved in the derivation of analytical solutions. First, the particle's trajectory has been approximated by $\mathbf{X}_t \approx \mathbf{X}_t^{(0)} + \mathbf{X}_t^{(1)}$ and higher-order terms $\mathbf{X}_t^{(n)}$, $n \geq 2$, have been

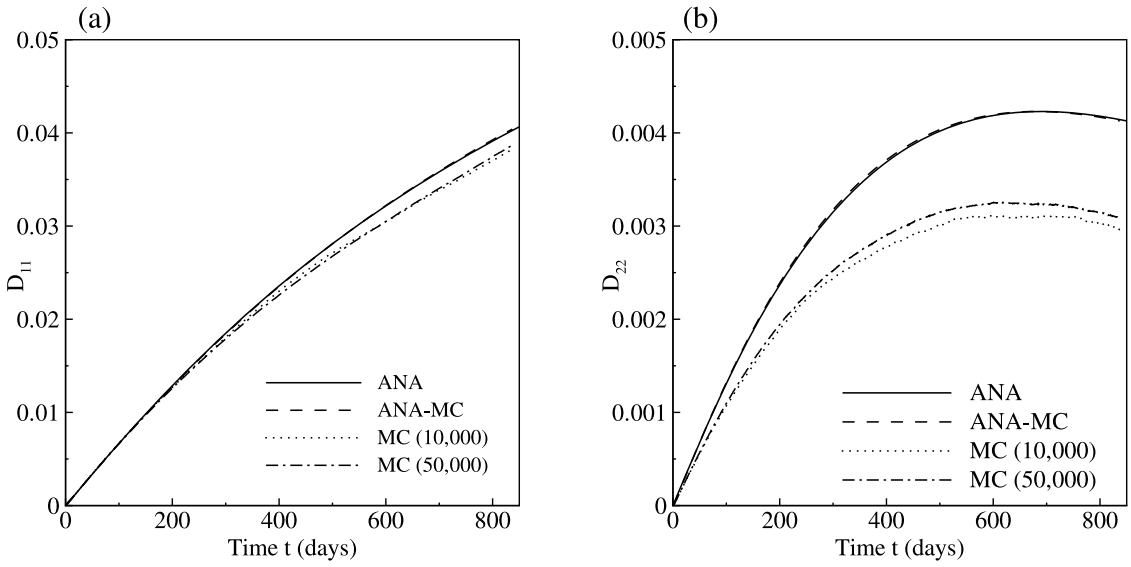

Figure 4. Comparison of time-dependent dispersivity: (a) D_{11} and (b) D_{22} derived from Monte Carlo simulations and the first-order analytical solutions.

truncated. In addition, $\mathbf{X}_t^{(1)}$ has been related to the velocity perturbation in (14) by approximating the actual position $\mathbf{X}_t$ using the zeroth-order term $\mathbf{X}_t^{(0)}$. Both of these approximations may introduce errors to the first-order solutions. To identify the dominating source of errors, we replace the position term $x_{01} + Ut$ in (19) and (20) at time t by the time-dependent mean position obtained from Monte Carlo simulations, and the results, labeled as ANA_MC, are also compared in both Figures 3 and 4. It seems that this correction does not improve the results. We may conclude that the discrepancy between Monte Carlo results and analytical solutions may be mainly due to neglecting higher-order terms in approximating $\mathbf{X}_t$.

[36] Although perturbation methods have been successfully applied in simulating flow in heterogeneous porous media with large variability, these methods in transport problems are usually limited to relatively small variability [*Morales-Casique et al.*, 2006b; *Liu et al.*, 2007]. The application of stochastic theories to problems with large variability σ_Y^2 is still a challenge. Our analytical solutions to displacement covariance and effective dispersivity are also limited to small variability of the log hydraulic conductivity fields.

3.2.2. Comparison With *Osnes*'s [1998] Solutions

[37] *Osnes* [1998] derived semianalytical solutions for displacement covariances X_{11} and X_{22} for the same problem as in this study, but his solutions are expressed as integrals of the velocity covariances, which in turns are presented as several complicated functions. This means that his solutions to X_{ij} need to be computed by numerical integration. In addition, his solutions were derived for isotropic porous media. In case 3, we try to reproduce Osnes's example [*Osnes*, 1998, Figure 6], in which he compared his solutions with Dagan's solutions [*Dagan*, 1984] for a rectangular domain of dimensionless size $L_1/\lambda = 20$ and $L_2/\lambda = 14$ with particles initially located at $(x_{01}/\lambda, x_{02}/\lambda) = (1, 7)$ and $(x_{01}/\lambda, x_{02}/\lambda) = (5, 7)$, respectively. It should be noted that for the case of isotropic hydraulic conductivity, analytical solutions depend on the dimensionless domain size and the actual size of the domain is irrelevant.

[38] Figure 5 compares the analytical solutions of dimensionless displacement covariances with solutions of *Osnes* [1998, see Figure 6]. Also compared in Figure 5 is the analytical solution from *Dagan* [1984] for unbounded domains. Figure 5 indicates that analytical solutions to X_{ij} presented in this paper is almost identical to those of *Osnes* [1998], but our solutions are much simple and are presented explicitly in terms of the statistics of the log hydraulic conductivity field. As observed by *Osnes* [1998], displacement covariance X_{11} computed from bounded domains is larger than its counterpart from unbounded domain, while it is opposite for X_{22}.

3.3. Characteristics of Solutions

[39] Upon investigating on the convergence and accuracy, it is appropriate to explore some general features of solute transport in bounded domains using the first-order analytical solutions.

3.3.1. General Features

[40] We start our discussion from the patterns of dimensionless displacement covariance X_{ii} and macrodispersivity D_{ii} as illustrated in Figures 1 and 2. Figure 1 shows that X_{11} increases almost linearly with time and X_{22} increases with time at a variable rate. Detailed variation of the rate can be better illustrated and explained using Figure 2, which is exactly the rate of change of X_{11} and X_{22} over time, because curves in Figure 2 are a half of the derivatives of the corresponding curves in Figure 1.

[41] It is interesting to see the differences between the macrodispersion coefficients for bounded and unbounded domains. The results for the latter are computed from the formulation of *Dagan* [1984]. It is seen from Figure 2 that the longitudinal macrodispersion coefficient D_{11} for unbounded domains has an asymptotic value at large dimensionless time and D_{11} is always smaller than that of bounded domains. A possible explanation is that while the lateral no-flow boundaries in bounded domains may limit the spreading of particles in the transverse direction, there is no such restriction in unbounded domains and therefore the macrodispersion coefficient D_{22} could be much large comparing to that in the

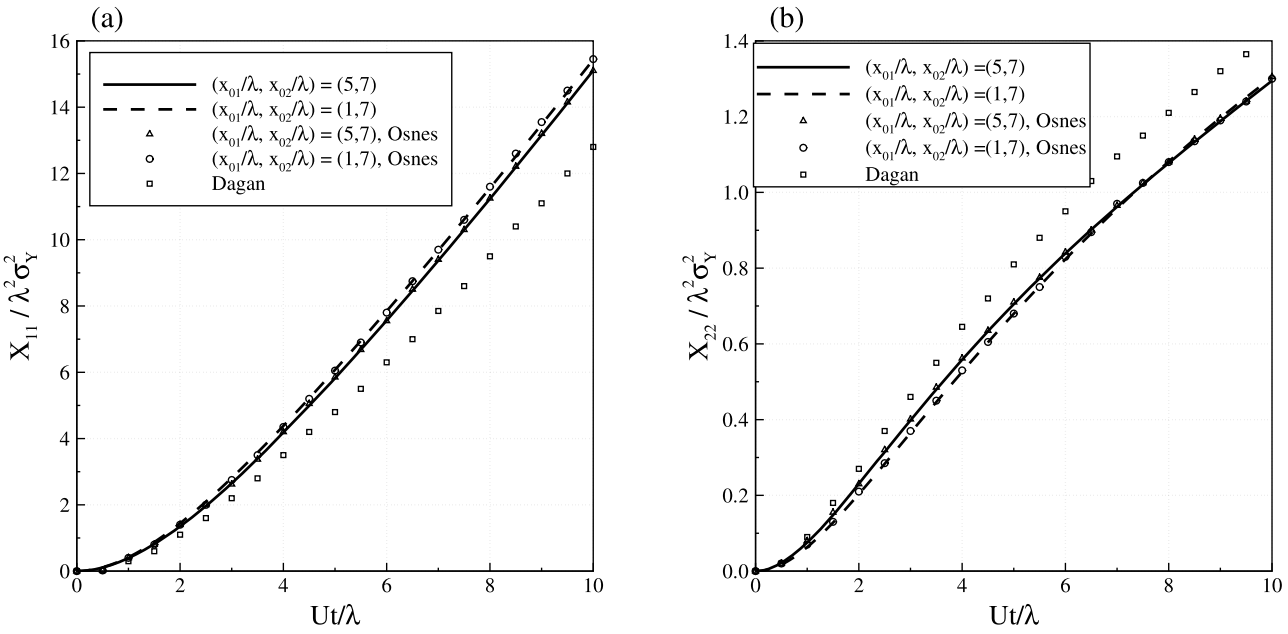

Figure 5. Comparison of time-dependent displacement covariances: (a) X_{11} and (b) X_{22} computed from (16)–(18) with those from *Osnes* [1998], for particles released at two different locations. For comparison purposes, solutions from *Dagan* [1984] for unbounded domains are also plotted.

bounded domains, which in turn may lead to smaller D_{11} in the unbounded domains.

[42] Figure 2a shows that the longitudinal effective dispersivity increases very fast at the beginning, then becomes more or less stabilized after the particles travel for about 5 correlation lengths, and increases again at later time when the particles are close to the downstream constant head boundary. This clearly indicates that (1) at the beginning X_{11} increases slowly (small values in the first segment of Figure 2a); (2) the continuing increase of D_{11} indicates that the plume always expands in the x_1 direction; and (3) at the later time when particles are close to the downstream constant head boundary, X_{11} increases at a relatively high rate, which will be explained later. The higher increase rate of X_{11} at later time has also been observed by *Morales-Casique et al.* [2006b], who evaluated numerically macrodispersivity using the moment methods for the unconditional case in which the longitudinal domain size is $12\lambda_Y$ [*Morales-Casique et al.*, 2006b, Figure 21].

[43] In the transverse direction (x_2), however, the pattern of the time-dependent D_{22} is quite different from that of D_{11}. First, although the size of plume in the transverse direction also expands over the time, the rate of expansion may decrease (see Figure 2b, $Ut/\lambda = 5\sim12.5$). In addition, there are two peaks on the curve as compared to the single peak for unbounded domains. The same pattern has also been discovered by *Morales-Casique et al.* [2006b] for the unconditional case with a longitudinal domain size of $12\lambda_Y$ [*Morales-Casique et al.*, 2006b, Figure 21]. All these features should be ascribed to boundary effects. Near the downstream boundary, the dimensionless effective dispersivity D_{22} is close to zero, which means that X_{22} stops increasing at this moment. The reason is that close to this boundary, the streamlines have to be perpendicular to the constant head boundary and the velocity component in the x_2 direction is zero. This may not be sufficient to explain quantitatively the patterns of D_{ii} curves, especially the time-dependent behaviors of D_{22}. Here we provide a more rigorous explanation.

[44] It is well known that macrodispersion D_{ii} can be derived directly from velocity covariances [*Dagan*, 1989]

$$D_{ii}(t) = \int_0^t u_{ii}(x_{01} + Ut', x_{02}; x_{01} + Ut, x_{02})dt'. \qquad (24)$$

As mentioned previously, because of nonstationarity of the velocity field, the integrand cannot be reduced to $u_{ii}(U(t-t'), 0)$ as in the case of infinite domains. In addition, because the arguments $(x_{01} + Ut', x_{02})$ and $(x_{01} + Ut, x_{02})$ of the integrand in (24) represent particle's mean positions at time t and t', respectively, this equation states that D_{ii} at time t is the cumulative effect of velocity covariance u_{ii} between the current position at time t and all points along particle's path ($t' < t$). For case 1 shown in Figures 1 and 2, we calculated a number of velocity covariance $u_{ii}(t, t')$, where both t and t' are dimensionless times, and plotted them in Figure 6. For instance, $u_{11}(15, t')$ stands for the covariance function between dimensionless time $t = 15$ and t', for all $t' \leq 15$. The area under this curve represents the value of D_{11} at dimensionless time $t = 15$. Note that the highest point on each of these covariance functions is the velocity variance at these points along the mean path, which in this case is along the line $x_2 = 250$ m because the particle was released at (0 m, 250 m). The velocity variances u_{11} and u_{22} along this line are illustrated in Figure 7, where squares and cycles on two curves represent the values that correspond to the highest values of curves in Figures 6a and 6b.

[45] Figure 6a shows that u_{11} is positive for all t, which, from (24), means that D_{11} always increases with time. Note that the velocity covariance $u_{ii}(t, t')$ is proportional to the velocity variance $\sigma^2_{uii}(t)$ along the path. It is easy to see from

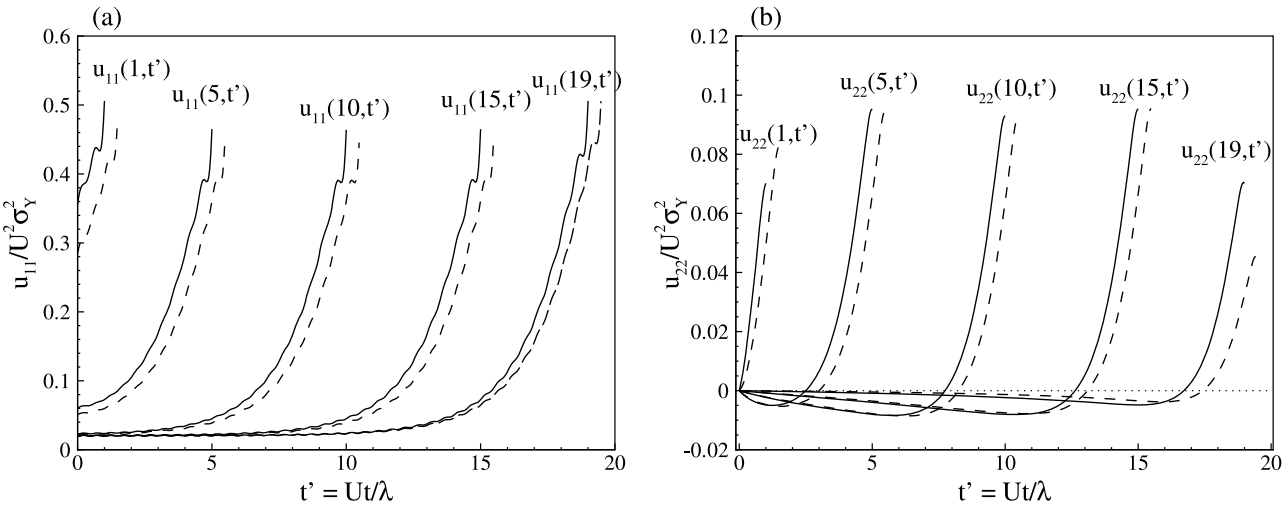

Figure 6. Velocity covariances computed from (8)–(10): (a) $u_{11}(t_1, t')$ and (b) $u_{22}(t_1, t')$ as a function of t' for some selected t_1.

Figure 6a that at the earlier time and the later time D_{11} increases faster. At the early time, although u_{11} decreases (see Figure 7), the increase of t, i.e., the interval of integral in (24), makes the value of integral increase quickly. At the later time, the faster increase of D_{11} is largely due to larger velocity variance when the particle travels close to the downstream boundary (see Figure 7).

[46] The feature of the velocity covariance function u_{22} is slightly different from that of u_{11}, as displayed in Figure 6b. The most important difference is that u_{22} (t, t') can be negative, which explains why D_{22} decreases in some time intervals. For example, the area under the curve u_{22} (5, t') is larger than that under the curve u_{22}(10, t'), which means that D_{22}(10) is smaller than D_{22}(5). Near the downstream boundary, velocity variance $\sigma_{u_2}^2$ approach zero (see Figure 7), so are the velocity covariance u_{22} (t, t') and macrodispersion coefficient D_{22} (t).

[47] It is interesting to see from Figure 7 that the velocity variances for bounded domains are significantly different from those of unbounded domains. For example, the variance of longitudinal velocity is larger than that for the unbounded domain (3/8), while the variance of the transverse velocity is slightly smaller than that for the unbounded domain (1/8).

3.3.2. Effects of Domain Sizes

[48] As mentioned earlier, the displacement covariances and effective dispersivity in a statistically anisotropic hydraulic conductivity field depend not only on the dimensionless domain size l_1 and l_2, but also on the aspect ratio of the domain $\epsilon = L_2/L_1$, as illustrated in (16)–(18), (22), and (23). This seems contradicting to Osnes's conclusion, which states that the effects of varying domain aspect ratio ϵ to the velocity covariance (and thus the displacement covariance and macrodispersivity) are small.

[49] To explore the effect of the domain size on displacement covariances and macrodispersivity, we compute a series of analytical solutions with a fixed length L_1 = 1000 m and a variable width L_2 = 100, 200, 300, 400, 500, 1000, 2000, and 5000 m. The correlation length is fixed in the x_1 direction at λ_1 = 10 m, while it varies in the x_2 direction in such a way that the dimensionless length in x_2 direction is fixed at L_2/λ_2 = 10. As a result, dimensionless sizes in two directions are fixed at L_1/λ_1 = 100 and L_2/λ_2 = 10.

[50] Figure 8 depicts the dimensionless displacement covariances as functions of dimensionless time for various values of the ratio ϵ. Figure 8a indicates that for $\epsilon < 1$, its value has little effect on dimensionless X_{11}. In fact, when $\epsilon = L_2/L_1$ varies in the range of 0.1 to 1, i.e., the length of the domain is as large as 10 times its width, X_{11} is almost unchanged (curves are almost overlapped). However, further increase of ϵ from 1 to 5 makes X_{11} change significantly. In particular, when ϵ is small, X_{11} increases at a relatively uniform rate. Intuitively, this seems correct, when the width is small (a narrow domain), dispersion of particles in the transverse direction is limited. When ϵ is large, dispersion in the longitudinal direction is slow at beginning because more dispersion in the transverse direction is allowed. Of particular interest phenomena is that at the final time when the downstream boundary is reached, X_{11} is a constant, regardless the aspect ratio of the domain. This may be explained mathematically using (16). Since α_m are solutions of equation $\sin(\alpha_m L_1) = 0$, and the particles are initially at ($x_{01} = 0, x_{02} = 250$ m), at the downstream boundary, both S_m (t) and S_{m1} (t) in (16) are zero. As a result, at this

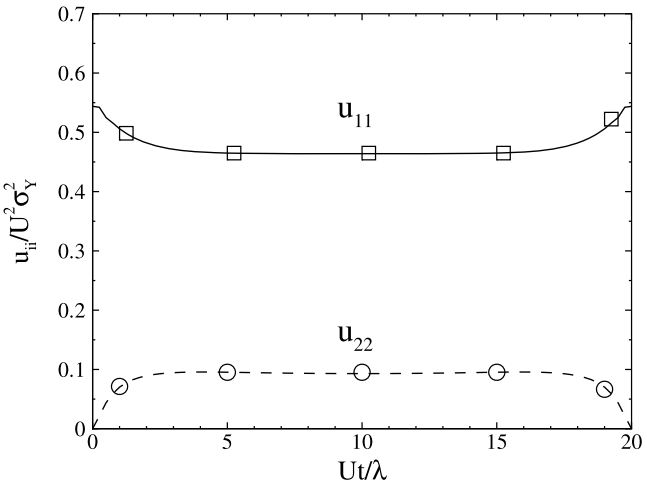

Figure 7. Velocity variances along $x_2 = L_2/2$. The squares and circles correspond to the highest points in Figures 6a and 6b, respectively.

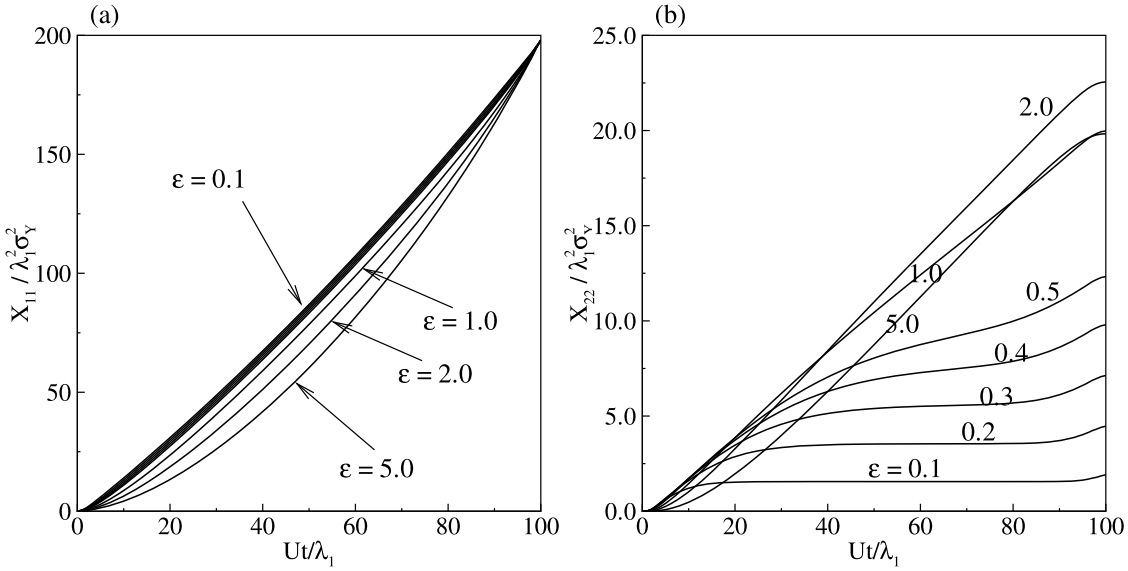

Figure 8. Time-dependent displacement covariances: (a) X_{11} and (b) X_{22} as functions of the domain aspect ratio $\epsilon = L_2/L_1$, for fixed dimensionless domain sizes $L_1/\lambda_1 = 100$ and $L_2/\lambda_2 = 10$.

boundary, only the third term in (16), which is independent of ϵ, contributes to X_{11}.

[51] The dependence of X_{22} on the aspect ratio is completely different from that of X_{11}, as shown in Figure 8b. For a small ϵ ($\leq$0.5), X_{22} increases quickly at the beginning, more or less stabilizes at a certain level that increases with ϵ, and then increases slightly near the downstream boundary. When $\epsilon < 1$, a larger ϵ in general leads to a larger X_{22}, because a larger width allows more space for particles to disperse in the transverse direction. Further increase of ϵ (i.e., $L_2 > L_1$) may lead to slow dispersion in the transverse direction at the early time. It is of interest to note that at a large ϵ, X_{22} increases almost linearly. This may imply that the nonlinear behavior of curves for $\epsilon < 1$ may be ascribed to the lateral boundaries that are perpendicular to the transverse direction.

[52] The effect of the domain aspect ratio ϵ on the normalized longitudinal and transverse macrodispersivities $\alpha_L = D_{11}/\lambda_1 U\sigma_Y^2$ and $\alpha_T = D_{22}/\lambda_1 U\sigma_Y^2$ are illustrated in Figure 9. When the aspect ratio is small, the longitudinal macrodispersivity increases very fast at the beginning and then increases linearly at a much slow rate until approaching the right boundary, where it increases again at a higher rate. For large ϵ (say, ϵ = 5.0), the longitudinal macrodispersivity increases almost linearly, and the boundary effect is relatively small. It seems that such behaviors of α_L represent the effect of lateral no-flow boundaries. The effect of domain aspect ratio ϵ on the transverse macrodispersivity α_T is completely different from that on α_L. When ϵ is smaller than one, α_T increases quickly at the early time and then decrease gradually because of limited space for particles to disperse in

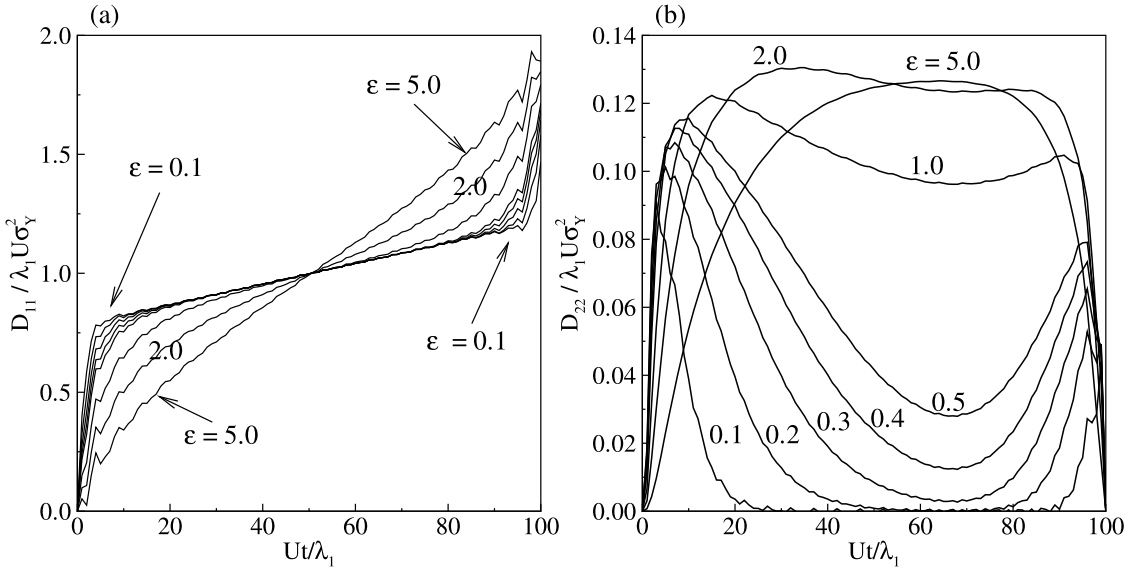

Figure 9. Time-dependent dispersivity: (a) D_{11} and (b) D_{22} as functions of the domain aspect ratio $\epsilon = L_2/L_1$, for fixed dimensionless domain size $L_1/\lambda_1 = 100$ and $L_2/\lambda_2 = 10$.

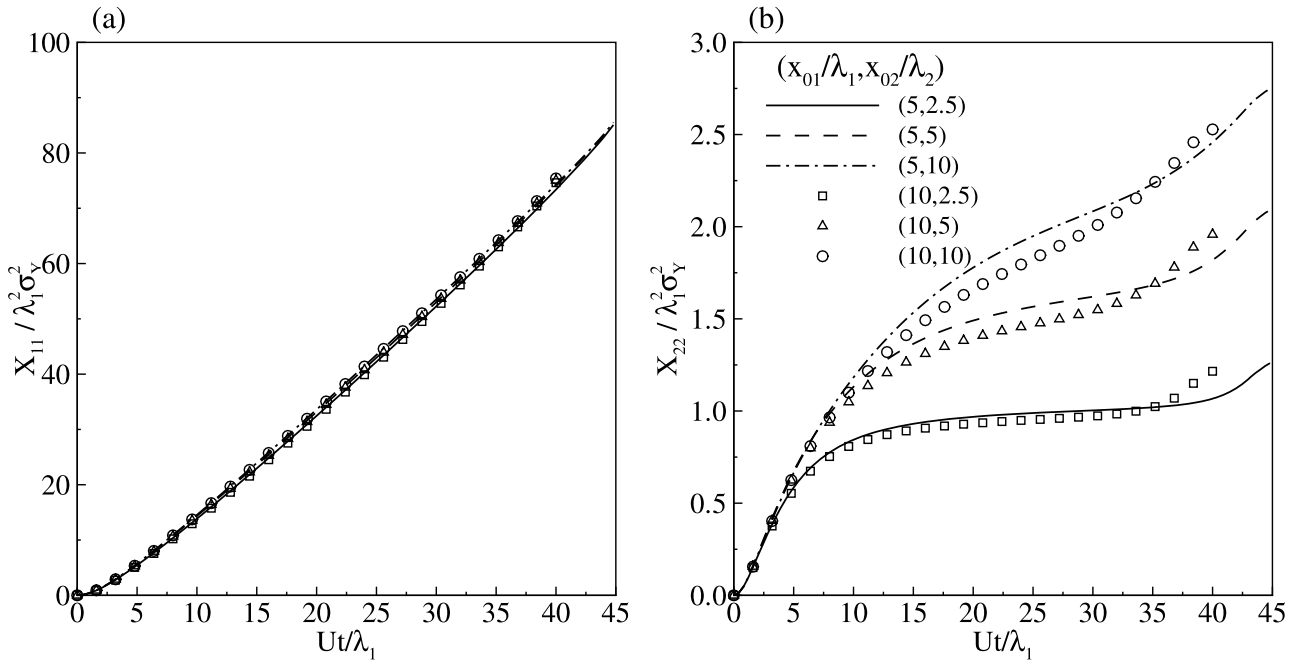

Figure 10. Dependence of dimensionless displacement covariances: (a) X_{11} and (b) X_{22} on particles' released locations.

the transverse direction. For a large ϵ, α_T keeps on increasing until the particle's mean position close to the downstream boundary, it then decreases because it has to be zero the downstream boundary.

3.3.3. Effect of Particles' Initial Locations

[53] *Osnes* [1998] claimed that the dependence of displacement covariances on the initial particle position is small. To investigate the effect of particles' release locations on the displacement covariances and macrodispersivities, X_{ii} and D_{ii} are computed for an array of initial locations in a domain of 1000 m × 500 m and correlation lengths of $\lambda_1 = \lambda_2 = 20$ m. Again, the similar boundary conditions as in the previous cases are adopted with constant heads of 10.5 m and 10.0 m at the left and right boundaries, respectively. This array of initial release locations includes 6 points resulted from combinations of $x_{01}/\lambda_1 = 5$ and 10, and $x_{02}/\lambda_2 = 2.5$, 5, and 10. Results are presented in Figures 10 and 11. Figure 10 indicates that the release location has little impact on the longitudinal displacement covariance X_{11}, as the curves with different release locations are almost overlapped. Different lengths of these curves are due to the variable total travel distance. In contrast to X_{11}, X_{22} is much more sensitive to the release location, as shown in Figure 10b. Comparison of two sets of curves with $x_{01}/\lambda_1 = 5$, and 10 indicates that the effect of x_{01} on the X_{22} is not significant, except that the boundary effect occurs earlier for the cases with $x_{01}/\lambda_1 = 10$ because of the short travel distance. The difference between these two sets of curves are even small when the release location is very close to one of the lateral boundaries (the solid line and squares, $x_{02}/\lambda_2 = 2.5$). However, for either $x_{01}/\lambda_1 = 5$ or 10, the effect of x_{02} is significant. In the cases that the release location is close to one of the lateral boundaries, the displacement covariance in the lateral direction is small, as the lateral boundary limits the dispersion in this direction. The latter cases are similar to the cases with a small aspect ratio ϵ discussed earlier. The sensitivity of X_{22} to the release location may be used to identify contaminant sources if boundaries are known, or to indicate some flow boundary conditions (i.e., presence of low permeable units). Similar observations can be made from Figure 11, which shows the dependence of dimensionless macrodispersivities on particles' initial locations.

4. Application to Borden Site

[54] Our analytical solutions, as most other similar solutions, are developed based on a number of assumptions. The assumptions include dimensionality of the problem and shape of the domain, appropriate boundary conditions, simplified flow scenarios (steady state, uniform mean flow), stationary permeability field with a separable exponential covariance function, and so on. As a consequence, the solutions are only applicable if the reality is not significantly away from these assumptions. It also makes it difficult to compare our model results against field or laboratory experimental results published in literature, as most of experiments were not designed for verifying stochastic models.

[55] In this section, we intend to apply our solutions to an unconfined sand aquifer at the Borden site, one of the most extensively studied sites [*MacKay et al.*, 1986; *Freyberg*, 1986]. The aquifer extends about 9 m beneath the nearly horizontal quarry floor and is underlain by a thick, silty clay deposit, which allows us to approximate the three-dimensional transport problem by a two-dimensional model. In fact, it has been found that the vertical spreading at the site is negligible [*Freyberg*, 1986]. This has also been supported by the finding that the vertical integral scale of the aquifer is much smaller than that in the horizontal plane [*Sudicky*, 1986]. Several studies showed that this assumption yield reasonably good results.

[56] There is a considerable amount of data in the literature regarding the statistics of the aquifer permeability and flow properties, although some of these data may be inconsistent.

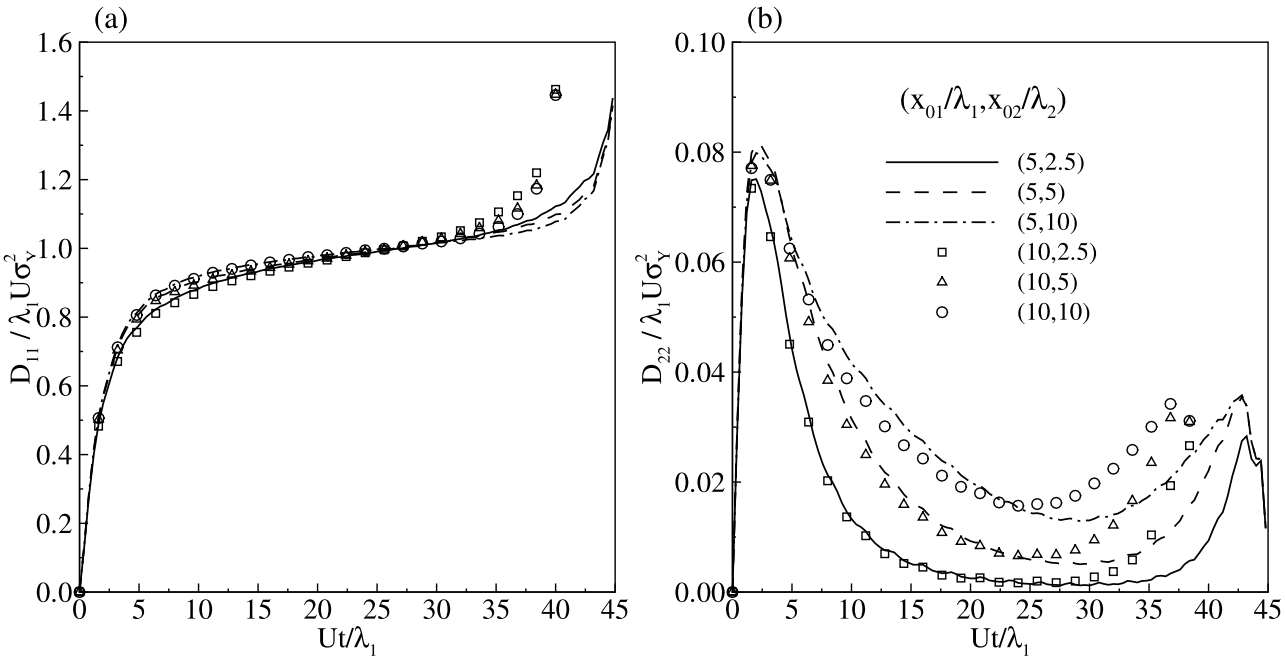

Figure 11. Dependence of dimensionless dispersivity: (a) D_{11} and (b) D_{22} on particles' released locations.

For example, the value of the horizontal integral scale was 2.7m in the work by *Freyberg* [1986], 2.8m in the work by *Naff et al.* [1988], and 5.14m in the work by *Bellin et al.* [1996]. Different values for the variance of the log conductivity have been used, and in some studies, this variance was adjusted by multiplying 0.74 because of the vertical average of the permeability field. In this studies, these parameters are taken as $\sigma_Y^2 = 0.172$ [*Bellin et al.*, 1996] and $\lambda_x = \lambda_y = 2.7$ m. The mean velocity is 0.091 m/d [*MacKay et al.*, 1986].

[57] Displacement covariance as a function of time was determined for two nonreactive species, bromite and chloride [*Freyberg*, 1986, Table 3]. We calculated apparent dispersivity values α_{11} and α_{22} from observed displacement covariances and the mean velocity. Because our model is only applicable to point sources, following *Freyberg* [1986], for nonzero initial displacement covariances, appropriate initial values have to be assigned: $X_{11}(0) = 1.8$ m^2 and $X_{22}(0) = 2.6$ m^2 [*Freyberg*, 1986].

[58] We assume the simulation domain is a rectangle of a size $L_1 = 400$ m and $L_2 = 200$ m, where x_1 is aligned with the mean flow direction. Displacement covariances derived from our solutions are compared in Figure 12 against the observed values. Though not perfect, the analytical solutions match the observed values reasonably well. If the averaged values of these tracers are used, as by *Freyberg* [1986], the match will be improved.

[59] Figure 13 compares macrodispersivities computed from our analytical solutions and those from observed dis-

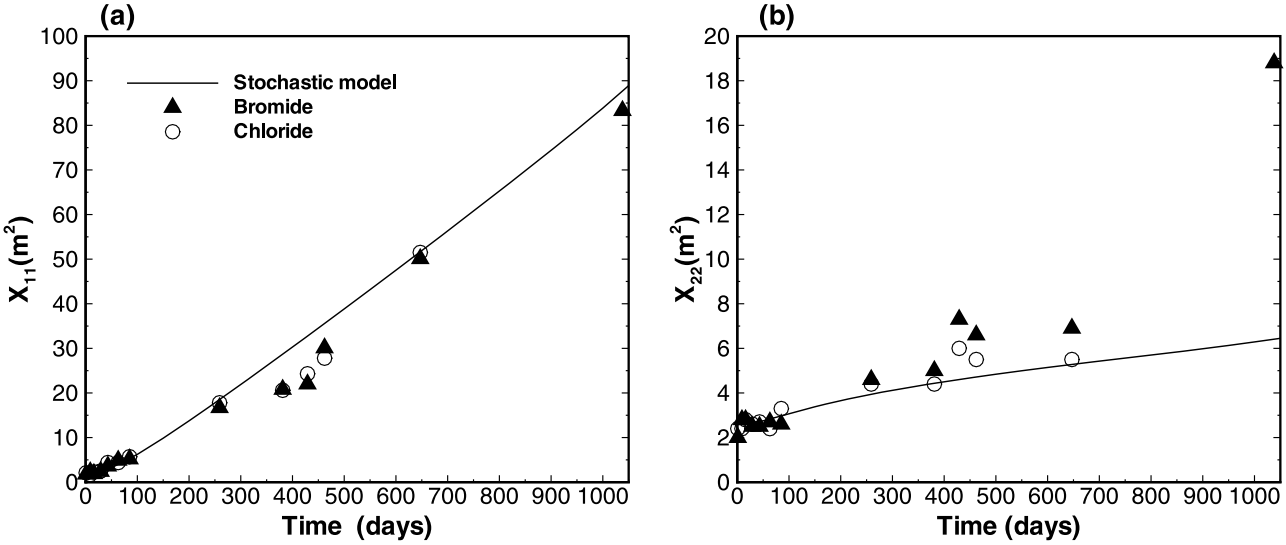

Figure 12. Comparison of displacement covariances computed from analytical solutions against observations: (a) X_{11} and (b) X_{22} for Borden site.

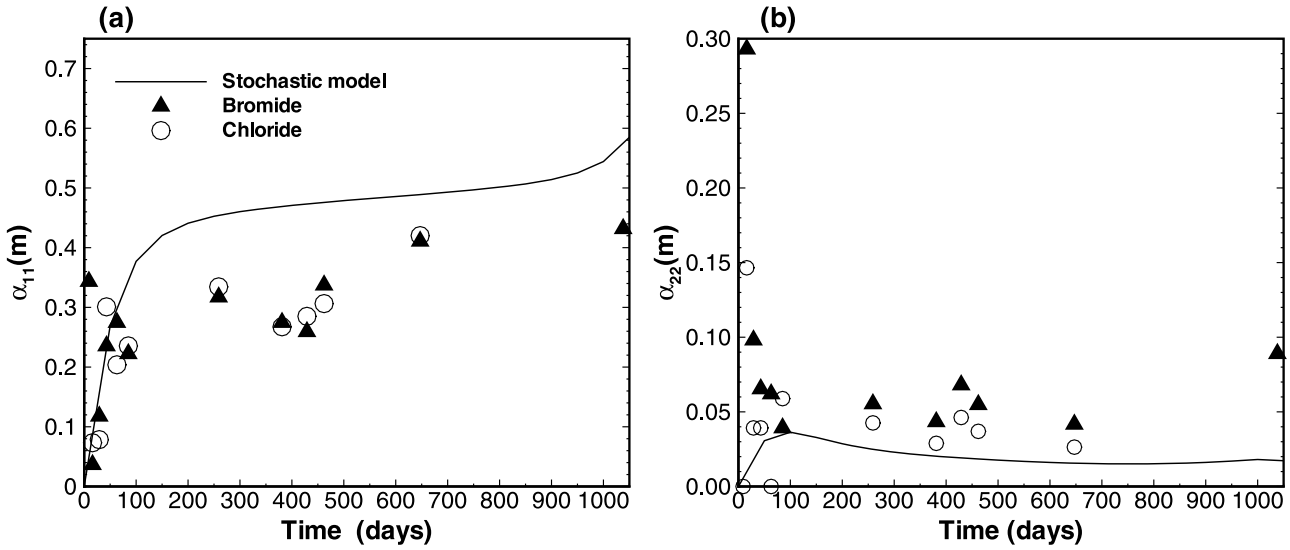

Figure 13. Comparison of dispersivity computed from analytical solutions against observations: (a) α_{11} and (b) α_{22} for Borden site.

placement covariances. The scale-dependent longitudinal macrodispersivities estimated from plume spreading increased from 0.06 at early time to 0.43 m. The asymptotic longitudinal macrodispersivity obtained from our analytical solution is 0.484m, which is almost the same as the value of 0.49m [*Freyberg*, 1986] and 0.50m [*Zhang and Neuman*, 1990; *Rajaram and Gelhar*, 1991]. The peak transverse macrodispersivity is about 0.04m, which is close to 0.05–0.06 m derived from plume moments [*Freyberg*, 1986; *Zhang and Neuman*, 1990; *Rajaram and Gelhar*, 1991].

5. Conclusions and Discussions

[60] In this study, we derived first-order analytical solutions to the displacement covariances X_{ij} and macrodispersion coefficients D_{ij} of conservative solute transport in two-dimensional, bounded heterogeneous porous media under uniform mean flow conditions. The solutions are explicitly related to statistics of the log hydraulic conductivity, such as its variance and correlation lengths.

[61] Because our analytical solutions are presented as infinity series, we first examined the convergence of these series in terms of the number of terms that have to be retained in the truncated finite summations. Our convergence study shows that although the rate of convergence depends on dimensionless domain size (the ratio of the domain size to the correlation length), in general, the longitudinal displacement covariance X_{11} converges faster than the transverse displacement covariance X_{22} does. In addition, X_{ij} converge faster than D_{ij} do. Furthermore, if all other parameters are the same, both X_{ij} and D_{ij} converge faster if the dimensionless domain size is small.

[62] The accuracy of the first-order solutions are assessed by comparing our solutions with the semianalytical solutions of *Osnes* [1998] and Monte Carlo simulations. The comparison shows that our solutions for the displacement covariances are almost identical to the results from Osnes's semianalytical solutions for the example illustrated in *Osnes* [1998] with isotropic conductivity fields. The comparison of the first-order solutions with the Monte Carlo results indicates that both X_{11} and D_{11} from analytical solutions are very close to Monte Carlo results, although relative large discrepancies are observed for X_{22} and D_{22}, especially at late time. Possible sources of such discrepancies have been investigated and it is concluded that the discrepancies may stem from the truncation of the higher-order terms, $\mathbf{X}_t^{(n)}$, $n \geq 2$, in approximating $\mathbf{X}_t$.

[63] The macrodispersivities for bounded domains are different from those for unbounded domains. Unlike in unbounded domains, the longitudinal macrodispersivity for bounded domains does not have an asymptotic value at large dimensionless time, and instead it increases quickly near the downstream constant head boundary. In addition, D_{11} for unbounded domains is always smaller than that in bounded domains, and accordingly, the transverse macrodispersivity D_{22} in unbounded domain is larger than that in bounded domain. The major mechanism for these differences is the effect of lateral no-flow boundaries in our bounded domain models.

[64] Some factors that controlling the macrodispersion have been investigated, including the domain aspect ratio and the particles' initial locations. It is important to note that X_{ij} and D_{ij} depends not only the dimensionless size of the domain, but also on its aspect ratio L_2/L_1. The dependence of X_{ij} and D_{ij} on the particles' initial location has been investigated at detail. Our results indicate that while this dependence is very small for X_{11} and D_{11}, the release location has a significant impact on both X_{22} and D_{22}. This contradicts to *Osnes*'s [1998, p. 212] conclusion that "the dependence of initial particle position on the displacement coefficients is shown to be small."

[65] The solutions are limited to two-dimensional rectangular domains with particular boundary conditions: constant head at two sides and no-flow conditions on lateral boundaries. It is possible to extend the solutions to three dimension cases, but expressions for both X_{ij} and D_{ij} will include sixfold summations, which reduces the convergence rate of the solutions. It is also possible to derive solutions for other types of boundary conditions by first solving the first-order flux covariance as in the work by *Lu and Zhang* [2005], and then

following the approach shown in this paper. Although in reality, flow and transport take place in three-dimensional space, in some cases they can be well approximated as two-dimensional flow. As demonstrated in section 4 using the data from the Borden site, the displacement covariances and macrodispersivity computed form analytical solutions are reasonably match the field observations, indicating that our solutions may be applicable to predict solute transport at the field scale, even though the assumptions on which the solution were derived may not be satisfied.

[66] Finally, it should be pointed out that in order to apply the results of the stochastic analysis to a field situation, it is necessary to invoke the ergodic hypothesis. This hypothesis refers to a condition at which a property of interest obtained from the space average is equivalent to that from the ensemble average. Though some studies indicate that macrodispersivity may significantly differ from realization to realization even after a few hundreds of heterogeneous scales [*Trefry et al.*, 2003], while other studies show that the macrodispersivity behaves ergodically at relatively small distances from the injection [*Jankovic et al.*, 2003; *Morales-Casique et al.*, 2006b]. Based on their nonlocal and localized analyses of nonreactive transport in bounded, heterogeneous porous media, *Morales-Casique et al.* [2006a, 2006b] showed that although solute transport in some cases may not be described by means of Fick's law with a constant or variable macrodispersion coefficient, under some conditions, the mean transport equation can be localized to yield an advection-dispersion equation with a macrodispersion tensor that varies generally in space-time. They illustrated several examples in which both the domain size and source size are relatively small. Interestingly, the patterns of D_{ii} [*Morales-Casique et al.*, 2006b, Figure 21] for the unconditional case with a domain size $12\lambda_Y \times 4\lambda_Y$ and source size of $0.8\lambda_Y \times 0.8\lambda_Y$ are the same as our corresponding patterns as shown in Figures 2 and 9.

[67] **Acknowledgment.** This work was partially supported by a Laboratory Directed Research and Development (LDRD) project (20070441ER).

References

Bellin, A., S. Salandin, and A. Rinaldo (1992), Simulation of dispersion in heterogeneous porous formations: Statistics, first-order theories, convergence of computations, *Water Resour. Res.*, *28*, 2211–2227.

Bellin, A., G. Dagan, and Y. Rubin (1996), The impact of head gradient transients on transport in heterogeneous formations: Application to the Borden site, *Water Resour. Res.*, *32*(9), 2705–2713.

Dagan, G. (1984), Solute transport in heterogeneous porous formations, *J. Fluid Mech.*, *145*, 151–177.

Dagan, G. (1987), Theory of solute transport by groundwater, *Annu. Rev. Fluid Mech.*, *18*, 183–215.

Dagan, G. (1988), Time-dependent macrodispersion for solute transport in anisotropic heterogeneous aquifers, *Water Resour. Res.*, *24*(9), 1491–1500.

Dagan, G. (1989), *Flow and Transport in Porous Formations*, Springer, New York.

Dagan, G. (1994), An exact nonlinear correction to transverse macrodispersivity for transport in heterogeneous formations, *Water Resour. Res.*, *30*, 2699–2705.

Dai, Z., A. V. Wolfsberg, Z. Lu, and R. W. Ritzi (2007), Representing aquifer architecture in macrodispersivity models with an analytical solution of the transition probability matrix, *Geophys. Res. Lett.*, *34*, L20406, doi:10.1029/2007GL031608.

Fiori, A. (1996), Finite Peclet extensions of Dagan's solutions to transport in anisotropic heterogeneous formations, *Water Resour. Res.*, *32*, 193–198.

Fiori, A. (1998), On the influence of pore-scale dispersion in nonergodic transport in heterogeneous formations, *Transp. Porous Media*, *30*, 57–73.

Freyberg, D. L. (1986), A natural gradient experiment on solute transport in a sand aquifer: 2. Spatial moments and the advection and dispersion of nonreactive tracers, *Water Resour. Res.*, *22*, 2031–2046.

Gelhar, L. W., and C. L. Axness (1983), Three-dimensional stochastic analysis of macrodispersion in aquifers, *Water Resour. Res.*, *19*(2), 161–180.

Gelhar, L. W., A. L. Gutjahr, and R. L. Naff (1979), Stochastic analysis of macrodispersion in a stratified aquifer, *Water Resour. Res.*, *15*, 1387–1397.

Gelhar, L. W., C. Welty, and K. R. Rehfeldt (1992), A critical review of data on field scale dispersion in aquifer, *Water Resour. Res.*, *28*(7), 1955–1974.

Guadagnini, A., and S. P. Neuman (1999a), Nonlocal and localized analyses of conditional mean steady state flow in bounded, randomly nonuniform domains: 1. Theory and computational approach, *Water Resour. Res.*, *35*(10), 2999–3018.

Guadagnini, A., and S. P. Neuman (1999b), Nonlocal and localized analyses of conditional mean steady state flow in bounded, randomly nonuniform domains: 2. Computational examples, *Water Resour. Res.*, *35*(10), 3019–3039.

Hsu, K.-C., D. Zhang, and S. P. Neuman (1996), Higher-order effects on flow and transport in randomly heterogeneous porous media, *Water Resour. Res.*, *32*, 571–582.

Jankovic, I., A. Fiori, and G. Dagan (2003), Flow and transport in highly heterogeneous formations: 3. Numerical simulations and comparison with theoretical results, *Water Resour. Res.*, *39*(9), 1270, doi:10.1029/2002WR001721.

Keller, A. A., P. V. Roberts, and P. Kitanidis (1995), Prediction of single phase transport parameters in variable aperture fracture, *Geophys. Res. Lett.*, *22*(11), 1425–1428.

Khan, A. U. H., and W. A. Jury (1990), A laboratory study of the dispersion scale effect in column outflow experiments, *J. Contam. Hydrol.*, *5*, 119–131.

Leland, D. F., and D. Hillel (1982), A field study of solute dispersion in a shallow, unconfined aquifer, *Soil Sci. Soc. Am. J.*, *46*, 905–912.

Li, H., and D. Zhang (2007), Probabilistic collocation method for flow in porous media: Comparisons with other stochastic methods, *Water Resour. Res.*, *43*, W09409, doi:10.1029/2006WR005673.

Li, S., and D. B. McLaughlin (1991), A nonstationary spectral method for solving stochastic groundwater problems: unconditional analysis, *Water Resour. Res.*, *27*(7), 1589–1605.

Li, W., Z. Lu, and D. Zhang (2009), Stochastic analysis of unsaturated flow with probabilistic collocation method, *Water Resour. Res.*, *45*, W08425, doi:10.1029/2008WR007530.

Liu, G., Z. Lu, and D. Zhang (2007), Stochastic uncertainty analysis for solute transport in randomly heterogeneous media using a Karhunen-Loève based moment equation approach, *Water Resour. Res.*, *43*, W07427, doi:10.1029/2006WR005193.

Lu, Z., and D. Zhang (2003), Solute spreading in nonstationary flows in bounded heterogeneous saturated-unsaturated media, *Water Resour. Res.*, *39*(3), 1049, doi:10.1029/2001WR000908.

Lu, Z., and D. Zhang (2005), Analytical solutions of statistical moments for transient flow in two-dimensional bounded, randomly heterogeneous media, *Water Resour. Res.*, *41*, W01016, doi:10.1029/2004WR003389.

MacKay, D., D. Freyberg, P. Roberts, and J. Cherry (1986), A natural gradient experiment on solute transport in a sand aquifer: 1. Approach and overview of plume movement, *Water Resour. Res.*, *22*(13), 2017–2029.

Morales-Casique, E., S. P. Neuman, and A. Guadagnini (2006a), Non-local and localized analyses of non-reactive solute transport in bounded randomly heterogeneous porous media: Theoretical framework, *Adv. Water Resour.*, *29*(8), 1238–1255.

Morales-Casique, E., S. P. Neuman, and A. Guadagnini (2006b), Nonlocal and localized analyses of nonreactive solute transport in bounded randomly heterogeneous porous media: Computational analysis, *Adv. Water Resour.*, *29*(9), 1399–1418.

Naff, R., T. C. Yeh, and M. Kemblowski (1988), A note on the recent natural gradient tracer test at the Borden site, *Water Resour. Res.*, *24*(12), 2099–2103.

Neuman, S. P., C. L. Winter, and C. M. Newman (1987), Stochastic theory of field-scale Fickian dispersion in anisotropic porous media, *Water Resour. Res.*, *23*(3), 453–466.

Osnes, H. (1995), Stochastic analysis of head spatial variability in bounded rectangular heterogeneous aquifers, *Water Resour. Res.*, *31*, 2981–2990.

Osnes, H. (1998), Stochastic analysis of velocity spatial variability in bounded rectangular heterogeneous aquifers, *Adv. Water Resour.*, *21*, 203–215.

Pang, L., and B. Hunt (2001), Solutions and verification of a scale-dependent dispersion model, *J. Contam. Hydrol.*, *53*, 21–39.

Porro, I., P. J. Wierenga, and R. G. Hills (1993), Solute transport through large uniform and layered soil columns, *Water Resour. Res.*, *29*, 1321–1330.

Rajaram, H., and L. W. Gelhar (1991), Three-dimensional spatial moments analysis of the Borden tracer test, *Water Resour. Res.*, *27*(6), 1239–1251.

Riva, M., A. Guadagnini, D. Fernandez-Garcia, X. Sanchez-Vila, and T. Ptak (2008), Relative importance of geostatistical and transport models in describing heavily tailed breakthrough curves at the Lauswiesen site, *J. Contam. Hydrol.*, *101*, 1–13.

Rubin, Y. (1990), Stochastic modeling of macrodispersion in heterogeneous media, *Water Resour. Res.*, *26*(1), 133–142.

Salandin, P., and V. Fiorotto (1998), Solute transport in highly heterogeneous aquifers, *Water Resour. Res.*, *34*(5), 949–961.

Sauty, J.-P. (1980), An analysis of hydrodispersive transfer in aquifers, *Water Resour. Res.*, *16*(1), 145–158.

Schwarze, H., U. Jaekel, and H. Vereecken (2001), Estimation of macrodispersion by different approximation methods for flow and transport in randomly heterogeneous media, *Transp. Porous Media*, *43*, 265–287.

Silliman, S. E., and E. S. Simpson (1987), Laboratory evidence of the scale effect in dispersion of solutes in porous media, *Water Resour. Res.*, *23*(8), 1667–1673.

Smith, L., and F. W. Schwartz (1980), Mass transport: 1. Stochastic analysis of macrodispersion, *Water Resour. Res.*, *16*(2), 303–313.

Sudicky, E. A. (1986), A natural-gradient experiment on solute transport in a sand aquifer: Spatial variability of hydraulic conductivity and its role in the dispersion process, *Water Resour. Res.*, *22*(19), 2069–2082.

Sudicky, E. A., J. A. Cherry, and E. O. Frind (1983), Migration of contaminants in groundwater at a landfill: A case study: 4. A natural-gradient dispersion test, *J. Hydrol.*, *63*, 81–108.

Taylor, S. R., and K. W. F. Howard (1987), A field study of scale-dependent dispersion in a sandy aquifer, *J. Hydrol.*, *90*, 11–17.

Trefry, M. G., F. P. Ruan, and D. McLaughlin (2003), Numerical simulations of preasymptotic transport in heterogeneous porous media: Departures from the Gaussian limit, *Water Resour. Res.*, *39*(3), 1063, doi:10.1029/2001WR001101.

Yeh, T.-C., L. W. Gelhar, and A. L. Gutjahr (1985), Stochastic analysis of unsaturated flow in heterogeneous soils: 1. Statistically isotropic media, *Water Resour. Res.*, *21*(4), 447–456.

Zhang, D., and Z. Lu (2004), An efficient, higher-order perturbation approach for flow in randomly heterogeneous porous media via Karhunen-Loève decomposition, *J. Comput. Phys.*, *194*(2), 773–794.

Zhang, D., and S. P. Neuman (1995), Eulerian-Lagrangian analysis of transport conditioned on hydraulic data: 1. Analytical-numerical approach, *Water Resour. Res.*, *31*(1), 39–51.

Zhang, D., and S. P. Neuman (1996), Effect of local dispersion on solute transport in randomly heterogeneous media, *Water Resour. Res.*, *32*, 2715–2723.

Zhang, R., K. Huang, and J. Xiang (1994), Solute movement through homogeneous and heterogeneous soil columns, *Adv. Water Resour.*, *17*, 317–324.

Zhang, Y.-K., and S. P. Neuman (1990), A quasi-linear theory of non-Fickian and Fickian subsurface dispersion: 2. Application to anisotropic media and the Borden site, *Water Resour. Res.*, *26*(5), 903–913, doi:10.1029/WR026i005p00903.

Zyvoloski, G. A., B. A. Robinson, Z. V. Dash, and L. L Trease (1997), Summary of the models and methods for the FEHM application—A finite-element heat- and mass-transfer code, *Rep. LA-13307-MS*, Los Alamos Natl. Lab., Los Alamos, N. M.

Z. Dai, Z. Lu, and A. V. Wolfsberg, Computational Earth Sciences Group, Los Alamos National Laboratory, Los Alamos, NM 87545, USA. (daiz@lanl.gov; zhiming@lanl.gov; awolf@lanl.gov)

C. Zheng, Department of Geological Sciences, University of Alabama, Tuscaloosa, AL 35487, USA. (czheng@ua.edu)